





# Interference between arsenic-induced toxicity and hypoxia

Vijay Kumar<sup>1,2</sup>  | Lara Vogelsang<sup>1</sup> | Thorsten Seidel<sup>1</sup> | Romy Schmidt<sup>3</sup> | Michael Weber<sup>4</sup> | Michael Reichelt<sup>5</sup> | Andreas Meyer<sup>6,7</sup>  | Stephan Clemens<sup>4</sup>  | Shanti S. Sharma<sup>2,8</sup> | Karl-Josef Dietz<sup>1</sup> 

<sup>1</sup>Department of Biochemistry and Physiology of Plants, Faculty of Biology, University of Bielefeld, Bielefeld, Germany

<sup>2</sup>Department of Biosciences, Himachal Pradesh University, Shimla, India

<sup>3</sup>Institute of Biology I (Botany/Molecular Genetics), RWTH Aachen University, Aachen, Germany

<sup>4</sup>Department of Plant Physiology, Faculty of Biology, Chemistry and Earth Sciences, University of Bayreuth, Bayreuth, Germany

<sup>5</sup>Department of Biochemistry, Max Planck Institute for Chemical Ecology, Jena, Germany

<sup>6</sup>Institute of Crop Science and Resource Conservation (INRES)-Chemical Signalling, University of Bonn, Bonn, Germany

<sup>7</sup>Bioeconomy Science Center, Forschungszentrum Jülich, Jülich, Germany

<sup>8</sup>Department of Botany, School of Life Sciences, Sikkim University, Gangtok, India

## Correspondence

Karl Josef Dietz, Department of Biochemistry and Physiology of Plants, Faculty of Biology, University of Bielefeld, 33615 Bielefeld, Germany.

Email: karl-josef.dietz@uni-bielefeld.de

## Funding information

Deutsche Forschungsgemeinschaft, Grant/Award Numbers: ME1567/9-1/2, RTG2064 and SPP1710; Indian Council of Medical Research; DAAD

## Abstract

Plants often face combinatorial stresses in their natural environment. Here, arsenic (As) toxicity was combined with hypoxia (Hpx) in the roots of *Arabidopsis thaliana* as it often occurs in nature. Arsenic inhibited growth of both roots and leaves, whereas root growth almost entirely ceased in Hpx. Growth efficiently resumed, and Hpx marker transcripts decreased upon reoxygenation. Compromised recovery from HpxAs treatment following reoxygenation indicated some persistent effects of combined stresses despite lower As accumulation. Root glutathione redox potential turned more oxidized in Hpx and most strongly in HpxAs. The more oxidizing root cell redox potential and the lowered glutathione amounts may be conducive to the growth arrest of plants exposed to HpxAs. The stresses elicited changes in elemental and transcriptomic composition. Thus, calcium, magnesium, and phosphorous amounts decreased in rosettes, but the strongest decline was seen for potassium. The reorganized potassium-related transcriptome supports the conclusion that disturbed potassium homeostasis contributes to the growth phenotype. In a converse manner, photosynthesis-related parameters were hardly affected, whereas accumulated carbohydrates under all stresses and anthocyanins under Hpx exclude carbohydrate limitation. The study demonstrates the existence of both synergistic since mutually aggravating effects and antagonistic effects of single and combined stresses.

## KEYWORDS

arsenic toxicity, *cis*-OPDA, ferredoxin, glutathione, hormones, hypoxia, redox sensors, redox signalling, stress combination, transcriptome

## 1 | INTRODUCTION

Plants are often exposed to multiple environmental stresses simultaneously (Mittler, 2002). Exposure to combinatorial stresses frequently alters the acclimation response. This may lead to both beneficial interactions, such as between hypoxia (Hpx) and aluminium stress (Ma, Zhu, Shabala, Zhou, & Shabala, 2016), and synergistic effects causing substantial losses in crop yield. Since long, plant survival and tolerance mechanisms have been studied in response to changes in single abiotic variables at a time (Mittler, 2002). Understanding of tolerance mechanisms is essential to utilize genetic engineering or smart breeding for crop improvement (Bohnert, Gong, Li, & Ma, 2006; Hirayama & Shinozaki, 2010).

Recent studies showed that plants do not necessarily respond to stress combinations in the same way as to individual stresses (Bankaji, Sleimi, López-Climent, Perez-Clemente, & Gomez-Cadenas, 2014; Rasmussen et al., 2013; Syvertsen & Garcia-Sanchez, 2014). Plants experiencing stress combinations show unique transcriptomic, proteomic, and metabolic changes (Pandey, Ramegowda, & Senthil-Kumar, 2015). The combination of drought with heat specifically affected >400 transcripts compared with the set of transcripts affected by drought or heat alone. Also, *Arabidopsis thaliana* accumulated sugars like sucrose and maltose as osmolytes under drought in the presence of heat, instead of proline, which increased in response to single drought stress (Rizhsky et al., 2004).

Likewise, heavy metal combinations, compared with exclusive exposure to Cu, Zn, or Cd individually, revealed both antagonistic and synergistic effects (Sharma, Schat, Vooijs, & Van Heerwaarden, 1999; Upadhyay & Panda, 2010). In some studies, single heavy metal stress enhances plant susceptibility to low concentrations of another less toxic metal ion (Sharma et al., 1999). In recent years, an increasing number of studies addressed plant responses to stress combinations (Prasch & Sonnewald, 2015). Understanding the underlying mechanisms for tolerance and sensitivity in the natural environment requires in-depth testing of stress combinations in laboratory experiments (Todgham & Stillman, 2013). Arsenic (As) and Hpx are two such environmental factors that have a deleterious effect on plant growth and can occur in nature simultaneously. It has been shown in barley roots that priming by Hpx improved cell viability under aluminium or low pH stress, probably by an enhanced antioxidative capacity (Ma et al., 2016).

The metalloid arsenic is an identified carcinogen and inhibits plant growth. Widespread contamination of groundwater and agricultural land exposes millions of people worldwide to As toxicity. For instance, groundwater As concentrations in Southeast Asia (Bengal basin; Bangladesh, Bengal) exceed the limits defined by the World Health Organization. Around 50 million lives are threatened (Zhao, McGrath, & Meharg, 2010). In plants, As(V) interferes with phosphate homeostasis and impairs processes like phosphate transport, protein phosphorylation, and ATP synthesis (Abercrombie et al., 2008; Catarecha et al., 2007; Tu & Ma, 2003).

As(V) is readily reduced by arsenate reductase to As(III) using glutathione (GSH) as reductant. As(III) reacts with thiols and thereby binds to protein sulphhydryl groups interfering with protein structure and function (Hughes, 2002). As(III) is sequestered by plants into the vacuole as phytochelatin (PC)-As(III) complexes (Song et al., 2010). Synthesis of PCs is strongly induced by arsenic through activation of PC synthase, GSH synthesis, and sulphur (S) metabolism (Schmöger, Oven, & Grill, 2000). As(III) also leads to generation of reactive oxygen species (ROS) and severe oxidative stress in plants due to lipid peroxidation (Sharma & Dietz, 2009; Srivastava, Ma, Singh, & Singh, 2005). ROS accumulation is critical because maintaining a steady state of ROS below the toxicity threshold is crucial to mediate efficient stress signalling (Mittler, Vanderauwera, Gollery, & Van Breusegem, 2004).

In the absence of active oxygen transport, oxygen gradients are established in plant tissues due to barriers for gaseous diffusion. Oxygen availability further deteriorates upon flooding and in compact soils. Hpx generates an energy crisis in plant cells and also inhibits other oxygen-dependent biochemical processes (Bailey-Serres & Voeselek, 2010; Lindsay & Maathuis, 2017). Low oxygen constraints plant growth and leads to losses of crop yield.

The primary challenge for plants under low oxygen is to maintain life-sustaining processes at the cost of accessory ones and to allocate the limited energy in an optimal manner (Shingaki-Wells, Millar, Whelan, & Narsai, 2014). Energy metabolism shifts to substrate level phosphorylation via glycolysis or anaerobic fermentation pathways for ATP generation in the absence of oxidative phosphorylation (Bailey-Serres & Voeselek, 2008; Van Dongen et al., 2008). Global changes in signalling patterns, transcript expression, synthesis of proteins, and primary and secondary metabolites are evident responses in hypoxic plants (Bailey-Serres & Chang, 2005).

Interestingly, even in low oxygen environments, ROS signalling plays a major role in inducing the acclimation response in plants (Steffens, Steffen-Heins, & Sauter, 2013). A fine balance between NADPH oxidases as generator of ROS and the ROS-scavenging system generates ROS signals, which bring about adaptation to hypoxic conditions (Blokhina & Fagerstedt, 2010; Poyton, Ball, & Castello, 2009).

Thus, arsenic as well as hypoxic growth conditions generates a characteristic signalling pattern, a significant part of which is mediated by ROS (Islam, Khan, & Irem, 2015; Pucciariello, Banti, & Perata, 2012). Oxidative bursts accompany As toxicity (Finnegan & Chen, 2012) and also participate in the ROS generation and ROS-mediated signalling for acclimation and tolerance under Hpx (Steffens et al., 2013). Arsenic tolerance in plants majorly depends on As complexation by PCs whose synthesis is S intensive. On the other hand, low oxygen in general impedes nutrient uptake and can affect S availability (Ernst, 1990). Hence, the similarities and dissimilarities between As stress and Hpx make the combination of these two stresses challenging for the plants.

Hpx and As stresses often occur simultaneously because under flooded conditions As(V) is reduced to As(III), and thus, As usually becomes much more available for plants. Therefore, the current work aimed to explore the effects of single and combined Hpx and As stresses applied at realistic stress levels to hydroponically grown *A. thaliana*. *A. thaliana* was chosen because many breakthroughs in the understanding of As detoxification were achieved with *Arabidopsis* (e.g., As(V) reductases and PC-As transporters).

To this end, marker transcripts and growth recovery were monitored to assess the reversibility of the severe inhibition under Hpx in both the presence and absence of As. To understand this response, the antioxidant network and the response of stress-specific markers were scrutinized. Intriguing observations concerned the rapid root to shoot signalling evident in form of effects of Hpx in roots on normoxia-exposed shoots, distinct effects of the stresses on ascorbate and thiol redox homeostasis, and the depletion of potassium as part of a comprehensive element analysis. Transcriptome analysis in roots revealed massive disturbance of potassium, sulphur, and redox homeostasis-related transcripts with synergistic and antagonistic responses.

## 2 | MATERIALS AND METHODS

### 2.1 | Plant growth and stress application

*A. thaliana* (Col-0; WT) and its Grx1-roGFP2 variant were grown hydroponically in 0.25 strength Hoagland's nutrient medium (1.25 mM KNO<sub>3</sub>, 0.5 mM (NH<sub>4</sub>)<sub>2</sub>H<sub>2</sub>PO<sub>4</sub>, 0.75 mM MgSO<sub>4</sub>, 1.50 mM Ca(NO<sub>3</sub>)<sub>2</sub> micronutrients, 14.5 μM Fe-EDTA, 500 μM MES, pH 5.25) for 32 days in 10-hr light (100 μmol m<sup>-2</sup> s<sup>-1</sup>) at 22/19°C (day/night temperature) and 50% relative humidity. The nutrient medium was renewed weekly and continuously aerated during the growth period (ambient air 21% O<sub>2</sub>). After 32 days of growth, plant roots were exposed to 250 μM As(V) (Na<sub>2</sub>HAsO<sub>4</sub>), to Hpx, or to the combination of both. The low oxygen state was established by transfer of the plants to new nutrient medium preflushed with air from a nitrogen generator for 48 hr (99.6% N<sub>2</sub> and 0.4% O<sub>2</sub>) to achieve immediate

hypoxic conditions. During the treatment, hypoxic conditions were maintained by continuous flushing (99.6% N<sub>2</sub> and 0.4% O<sub>2</sub>) for hypoxic and combination treatment, while control plants were aerated as before (21% O<sub>2</sub>). The shoots remained in air under control light conditions. Reaeration was started by transferring the plants to nutrient medium aerated with 21% O<sub>2</sub> similar to the control conditions for 3 weeks.

The O<sub>2</sub> content of the media was determined daily using a Clark-type oxygen electrode. The average O<sub>2</sub> concentration ( $M \pm SE$ ,  $n = 15$  experiments) of the growth media was  $262 \pm 6.8 \text{ nmol ml}^{-1}$  for control and As, and  $86 \pm 4.3 \text{ nmol ml}^{-1}$  for Hpx and HpxAs. The oxygen content remained stable over the 7-day treatment period in control as well as in the hypoxic growth media. Plant material was harvested after 7 days of treatment and 4 hr and 3 weeks of reaeration. The harvested plant material was either weighed for growth measurement or grinded in liquid N<sub>2</sub> and stored at  $-80^\circ\text{C}$ .

## 2.2 | Photosynthesis-related parameters and pigments content

Photosystem II (PSII) quantum yield was measured with the Photosynthetic Yield Analyzer (Mini-PAM, Walz, Germany) as  $(F_m - F_o)/F_m$ , with  $F_o$  and  $F_m$  being the minimum and maximum values of chlorophyll fluorescence for dark-adapted leaves (Motohashi & Myouga, 2015). The amount of photosystem I (PSI; P700) and the redox state of ferredoxin (Fdx) were analysed in intact leaves using the Dual/KLAS-NIR 100 (kinetic LED array spectrophotometer near infrared; Klughammer & Schreiber, 2016; Schreiber, 2017; Schreiber & Klughammer, 2016). Parameters were measured either before the start of the light period or after 1-hr dark adaptation.

Chlorophyll (extract in 80% acetone) and anthocyanin contents (extract in MeOH with 1% HCl) were measured photometrically. Their amounts were determined using the following equations (Lichtenthaler & Buschmann, 2001; Rabino & Mancinelli, 1986):

$$Chl_a \left( \mu\text{g ml}^{-1} \right) = 12.25A_{663\text{nm}} - 2.79A_{645\text{nm}}, \quad (1)$$

$$Chl_b \left( \mu\text{g ml}^{-1} \right) = 21.50A_{645\text{nm}} - 5.10A_{663\text{nm}}, \quad (2)$$

$$\text{Anthocyanin}_{\Delta A} = A_{530\text{nm}} - 0.25A_{657\text{nm}}. \quad (3)$$

## 2.3 | Microarray and quantitative transcript analysis

Plant tissues were pulverized in liquid nitrogen and stored at  $-80^\circ\text{C}$ . RNA was isolated using the LiCl precipitation method. Cells were extracted with 750  $\mu\text{l}$  of Tris buffer (100 mM; pH 7.8) containing sodium dodecyl sulphate (SDS; 4%), NaCl (600 mM), and EDTA (20 mM) and 750  $\mu\text{l}$  phenol:chloroform:isoamylalcohol (PCI; 25:24:1). After shaking for 30 min, the samples were centrifuged (16,000 $\times$ g, 20 min). The collected uppermost layer was cleared by adding 750  $\mu\text{l}$  PCI to remove proteins and other metabolites, leaving behind nucleic acids. After centrifugation, RNA was precipitated by adding 8 M LiCl (0.75 volume of the sample) and incubation overnight at  $4^\circ\text{C}$ . The RNA pellet was resuspended in autoclaved distilled water (200  $\mu\text{l}$ ). After addition of

50  $\mu\text{l}$  sodium acetate (3 M, pH 5.2) and 1 ml EtOH (96%,  $-20^\circ\text{C}$ ), the samples were incubated at  $-80^\circ\text{C}$  for 1 hr. RNA precipitates collected after centrifugation were washed two times with 70% EtOH ( $-20^\circ\text{C}$ ) to remove salts. The precipitates were dried at  $56^\circ\text{C}$  and dissolved in RNase-free water at  $56^\circ\text{C}$  with shaking. Quantity and quality of the RNA were tested with the NanoDrop ND-1000 spectrophotometer and by gel electrophoresis (Aranda, LaJoie, & Jorcyk, 2012).

Root RNA was used for microarray hybridization. RNA quality was tested prior to hybridization using the Agilent 2100 Bioanalyzer system. All samples had RNA integrity numbers  $\geq 9$ . Sample preparation was carried out as described in the Affymetrix GeneChip WT PLUS manual (Affymetrix, Inc., Santa Clara, CA). In brief, double-stranded cDNA synthesized from 200 ng of total RNA was used for cRNA synthesis; 12  $\mu\text{g}$  cRNA was purified and reverse transcribed into sense-strand (ss) cDNA containing synthetic dUTP residues. Purified ss cDNA was fragmented using a combination of uracil DNA glycosylase and apurinic/apyrimidinic endonuclease 1 (APE 1) followed by a terminal labelling with biotin; 3.8  $\mu\text{g}$  of fragmented and labelled ss cDNA was hybridized to Affymetrix Arabidopsis Gene 1.0 ST arrays for 16 hr at  $45^\circ\text{C}$  in a GeneChip Hybridization Oven 640. Hybridized arrays were washed and stained in an Affymetrix Fluidics Station FS450, and the fluorescent signals were measured with an Affymetrix GeneChip Scanner 3000 7G. Fluidics and scan functions were controlled by the Affymetrix GeneChip Command Console v4.1.3 software. Sample processing was performed at an Affymetrix Service Provider and Core Facility, "KFB-Center of Excellence for Fluorescent Bioanalytics" (Regensburg, Germany; www.kfb-regensburg.de). The array data were deposited at GEO-NCBI and are available with the accession number GSE119327.

Summarized probe set signals in Log<sub>2</sub> scale were calculated by using the RMA (Irizarry et al., 2003) algorithm with the Affymetrix Gene Chip Expression Console v1.4 Software. The generated ".cel" files were analysed further using the Expression Console Version 1.4.1 (Affymetrix) and Transcriptome Analysis Console Version 3.1 (Affymetrix). Average signal values from three independent experiments were evaluated; sample sets with a fold change  $> 2$  and  $p$  value  $< 0.05$  were considered as significantly regulated. Venn diagrams were prepared using the online tool Draw Venn Diagram (bioinformatics.psb.ugent.be/webtools/Venn/).

RNA samples were processed to generate cDNA for qRT-PCR by using MMLV reverse transcriptase in presence of RNasin (Promega). Transcripts were quantified on MyiQ (Bio-Rad) using KAPA SYBR qPCR Master Mix. qRT-PCR primers (Table S1) were designed using Primer3Plus (www.bioinformatics.nl/cgi-bin/primer3plus/primer3plus.cgi; Untergasser et al., 2007) and tested to exclude unspecific binding in *Arabidopsis* Refseq mRNA database using NCBI Primer-BLAST (Ye et al., 2012). The programme for qRT-PCR consisted of 5 min  $95^\circ\text{C}$ , 15 s  $95^\circ\text{C}$ , annealing (specified for different primer pairs) 30 s, and 45 s  $72^\circ\text{C}$ . The melt curve consisted of a ramp from  $55^\circ\text{C}$  to  $95^\circ\text{C}$ . PCR efficiency and amplification curves for different target genes were analysed using LinRegPCR 11.0 software (Ramakers, Ruijter, Deprez, & Moorman, 2003; Ruijter et al., 2009). Gene expression was normalized by calculating the normalization factor from the geometric mean of actin (*ACT2*) and tubulin (*TUB5*) expression as described by Vandesompele et al. (2002).

## 2.4 | Gene Ontology enrichment analysis and heat diagrams

The transcriptome data were analysed for enrichment of biological process-related Gene Ontology (GO) terms using the online GO classification tool PANTHER7 (<http://www.pantherdb.org/>; Mi et al., 2009; Thomas et al., 2003). The transcripts specifically responding to HpxAs were mapped into different categories related to cell metabolism and transport using the MapMan tool (Thimm et al., 2004). Heat diagrams were developed using HeatMapper (<http://www.heatmapper.ca/>; Babicki et al., 2016).

## 2.5 | Ratiometric analysis of in vivo GSH redox potential

The cytosolic GSH redox potential ( $E_{\text{GSH}}$ ) in root cells was measured ratiometrically with a confocal laser scanning microscope (LSM 780, Carl Zeiss, Germany). The 405-nm laser diode (30 mW) and the argon multiline laser (488 nm, 25 mW) were used with corresponding main beam splitters to excite roGFP2 at both characteristic excitation bands. roGFP2 emission was recorded between 500 and 530 nm. At 10 $\times$  magnification (Zeiss Plan-Apochromat 10x/0.45 M27) with a pixel dwell time of 1.2–2.2  $\mu$ s and a data depth of 12 bits per pixel, seven to 10 images were recorded per treatment per time point in line-switching mode. The signal-to-noise ratio was optimized by adjusting the gain (master) and pinhole for different images. DTT and H<sub>2</sub>O<sub>2</sub> (10 mM each) were administered at the end of the measurement to get fluorescence intensities for completely reduced and oxidized roGFP2, respectively. Images were evaluated with the ZEN software for fluorescence intensities of oxidized and reduced roGFP2.

Fluorescence intensities for both excitation channels were collected separately from three different regions of interests (ROIs) within the meristematic zone in the root apex. Background noise was below 1% and, thus, negligible. The ratio  $R_t$  was calculated for each ROI (region of interest) based on the mean intensities of the two channels. Calculations per treatment and time point were carried out for seven to 10 independent root images. The ratios allowed for calculation of the degree of oxidation (OxD) of each image based on Equation 4 (Schwarzländer et al., 2008).

$$\text{OxD}_{\text{roGFP2}} = \frac{R_t - R_{\text{red}}}{\frac{I_{488\text{ox}}}{I_{488\text{red}}}(R_{\text{ox}} - R_t) + (R_t - R_{\text{red}})}, \quad (4)$$

where  $R_t$  gives the fluorescence ratio at 405/488 nm and  $R_{\text{red}}$  and  $R_{\text{ox}}$  are ratios for completely reduced or oxidized roGFP2. Further,  $I_{488\text{red}}$  and  $I_{488\text{ox}}$  are the intensities at 488 nm for fully reduced and fully oxidized roGFP2, respectively. The  $E_{\text{GSH}}$  was estimated by inserting the OxD in the derived Nernst equation as shown in Equation 5:

$$E_{\text{GSH}} = E_{\text{roGFP2}} = E_{\text{roGFP2}}^{\text{pH}} - \frac{RT}{zF} \ln \left[ \frac{1 - \text{OxD}_{\text{roGFP2}}}{[\text{OxD}_{\text{roGFP2}}]} \right], \quad (5)$$

where  $R$  is the gas constant (8.315 J K<sup>-1</sup> mol<sup>-1</sup>),  $T$  the absolute temperature (298.15 K),  $z$  the number of transferred electrons (2), and  $F$  the Faraday constant (9.648  $\times$  10<sup>4</sup> C mol<sup>-1</sup>). The redox potentials of GSH ( $E_{\text{GSH}}$ ) depend on OxD of the respective redox pair.  $E_{\text{roGFP2}}^{\text{pH}}$

is the midpoint redox potential of roGFP2 based on the standard midpoint potential at pH 7 corrected for the estimated cytosolic pH of 7.2 (Equation 6):

$$E_{\text{roGFP2}}^{\text{pH}} = E_{\text{roGFP2}}^{\text{O}'} - 60.1 \text{ mV} (\text{pH} - 7), \quad (6)$$

where  $E_{\text{roGFP2}}^{\text{O}'}$  was set to -280 mV previously suggested as consensus midpoint redox potential by Hanson et al. (2004). The pH corrected  $E_{\text{roGFP2}}^{\text{pH}}$  of -292.02 mV was used in Equation 6 to calculate kinetics of stress-specific  $E_{\text{GSH}}$ .

To visualize differences in  $E_{\text{GSH}}$ , ratiometric images from the two channels (excitation with 405 and 488 nm) were calculated (ZEN software black edition, Carl Zeiss microscopy).

## 2.6 | Biochemical and physiological parameters

Nonprotein thiols, GSH, and ascorbate were determined in freshly harvested tissues, which were grinded in liquid nitrogen within 24–48 hr. In the meantime, plant tissues were stored at -80°C if needed. Nonprotein thiols were measured with 5,5'-dithiobis-(2-nitrobenzoic acid) (DTNB), which releases one 2-nitro-5-thiobenzoate per one thiol and can be detected spectrophotometrically at 412 nm. Acidic extraction in 0.2 N HCl with 1 mM EDTA ensured precipitation of proteins. GSH standard was used for calculation. Sample absorption at 412 nm was subtracted to get the DTNB-specific absorbance.

GSH and ascorbate redox state and contents were measured with the plate reader assay described by Queval and Noctor (2007). Leaf and root tissues were extracted with 0.2 N HCl followed by neutralizing with 0.2 N NaOH. GSH was specifically determined with GSH reductase (EC 1.6.4.2) along with its substrate NADPH in the presence of DTNB at 412 nm. To determine the content of GSH disulphide (GSSG), one part of the neutralized extract GSH (reduced GSH) was blocked by using 2-vinyl pyridine. GSH (0–0.90 nmol) and GSSG (0–0.18 nmol) standards were used for calculating amounts.

Ascorbate was measured in the neutralized extract using ascorbate oxidase (AO). The decrease in absorbance at 265 nm was determined 2 min after AO addition. The subtraction of initial absorbance for leaf extracts and the final absorbance after 2 min of AO addition gave the ascorbate-specific absorbance change. Total ascorbate was measured after treating the neutralized leaf extract with DTT (1 mM), whereas the samples without DTT quantified the reduced fraction. Oxidized ascorbate was calculated from total minus reduced ascorbate amounts. Calculations were based on the corrected extinction coefficient for ascorbate (7,000 M<sup>-1</sup> cm<sup>-1</sup>) for the 96-well plate (Queval & Noctor, 2007).

Soluble and insoluble sugars were measured with the anthrone assay (Yemm & Willis, 1954). Plant tissues (20–30 mg) were homogenized with 1 ml EtOH (80%) and incubated at 50°C for 10 min. The samples were centrifuged and the resulting supernatant was used for measurement of soluble sugars. The washed pellet was suspended in 1 ml HCl (1 N) and incubated at 95°C for 1 hr to hydrolyse the insoluble carbohydrates. Further centrifugation provided the supernatant for measurement of insoluble sugars. Sugars were quantified spectrophotometrically as furfural derivative-anthrone complex at 620 nm.



The sugar extract from the plant tissues (30–50  $\mu\text{l}$ ) was mixed with 970  $\mu\text{l}$  of anthrone reagent (40% anthrone in 75%  $\text{H}_2\text{SO}_4$  supplemented with 0.4% of thiourea) and incubated at 95°C for 15 min. The absorbance of the samples at 620 nm was compared with that of a glucose standard (0–30  $\mu\text{g}$ ).

Hydrogen peroxide contents were measured in freshly prepared samples with a luminol-based assay as described by König et al. (2014).

## 2.7 | Immunological detection of redox status of PrxIIIF

PrxIIIF amounts and redox state were assessed by Western blot. Proteins were extracted from stored (–80°C) samples in Tris buffer (120 mM, pH 6.8) with or without mPEG<sub>5000</sub>-maleimide (methoxypolyethylene glycol maleimide; mass shift of 5 kDa). Protein was quantified in the supernatant (Bradford, 1976). Protein equivalent to 10  $\mu\text{g}$  was mixed with DTT (100 mM) to reduce all disulphides (oxidized thiols) and further incubated at 95°C with SDS (5%) containing protein-loading buffer for 10 min to denature the proteins. These samples were run on SDS-polyacrylamide gel electrophoresis, and proteins blotted on nitrocellulose membrane. The membrane was incubated with PrxIIIF specific antibody. The secondary antibody was used as horseradish peroxidase conjugate. The signal was detected through chemiluminescence on X-ray films (König et al., 2014).

## 2.8 | Elemental analysis and measurement of hormonal content

Element contents were quantified in leaves or roots washed in ice-cold buffer (1 mM  $\text{K}_2\text{HPO}_4$ , 0.5 mM  $\text{Ca}(\text{NO}_3)_2$ , 5 mM MES, pH 5.6) for 30 min to remove traces of surface adsorbed As. The samples were dried at 80°C, acid digested (5–150 mg in 2 to 4 ml of 65%  $\text{HNO}_3$  supplemented with 1 to 2 ml of 30%  $\text{H}_2\text{O}_2$ ) at 80°C for 10 min, and subsequently heated to 180°C for 16 min in a microwave oven. The metal contents were measured by inductively coupled plasma-optical emission spectrometry using the following wavelength: Ca 396.8 nm, K 766.4 nm, Mg 279.0 nm, P 185.9 nm, S 182.0 nm, As 189.0 nm, and Mg 285.2 nm. Hormone levels (ABA, JA, JA-Ile, *cis*-OPDA, and JA) were determined by LC-MS/MS from the undiluted methanol extract prepared as described by Vadassery et al. (2012) using an API 5000 mass spectrometer (Applied Biosystems).

## 2.9 | Statistical analysis

Data are presented as means with standard error. Statistical analysis (one-way and two-way analysis of variance followed by Tukey's post hoc test) was performed to evaluate significant differences among means using IBM SPSS Statistics 20 (IBM, 2011). Significantly different means ( $p < 0.05$ ) are marked with different letters, whereas missing letters indicate lack of significance.

## 3 | RESULTS

### 3.1 | Plant growth and phenotypes

Hydroponically grown 32-day-old *A. thaliana* plants were treated with 250  $\mu\text{M}$  As, or the nutrient medium was flushed with 0.4%  $\text{O}_2$ , compared with 21%  $\text{O}_2$  under control conditions to establish root Hpx, or exposed to the combination of both for 7 days (Figure 1a). Plants subjected to Hpx were subsequently re-aerated with 21%  $\text{O}_2$ . The plants continued to grow in the presence of As, albeit at a reduced rate. In a converse manner, root growth essentially ceased in hypoxic environment, whereas the rosettes still showed some biomass increase (Figure 1b). Root growth was inhibited in the presence of the combined stresses similarly as in single Hpx stress. However, rosette growth was more inhibited in the combined treatment, indicating some additional interference or additive inhibitory effects. The severity of the stress-induced disorder after 7 days of stress was investigated by re-aeration of the hydroponic medium (Figure 1c). Both root and rosette growth recovered during re-aeration from previous Hpx and combined stresses. Efficient recovery was particularly evident for the Hpx-treated plants and demonstrates the transient nature of growth arrest in low  $\text{O}_2$ , which was readily overcome upon resupply of adequate  $\text{O}_2$ . However, presence of arsenic impeded the growth recovery of roots if combined with Hpx.

### 3.2 | Transcript response of stress marker genes

To dissect the responses of roots and rosettes in detail and to address involved mechanisms, we first analysed the response of marker transcripts and then scrutinized the global transcriptome response.

Changes in marker transcript levels revealed the expected strong increases in Hpx markers such as *alcohol dehydrogenase 1 (ADH1)*, *hypoxia response attenuator 1 (HRA1)*, and *stearoyl acyl carrier protein desaturase 9 (HUP9)*; (Figure 2a). The maximum fold change among these markers was 7,100-fold for *HUP9* in roots. After re-aeration of the Hpx-exposed plants, each of these transcripts decreased within 4 hr; for example, *HUP9* dropped from 7,100 to 21 relative units. *ADH1* and *HRA1* showed a small increase also in leaves, albeit they were not exposed to Hpx (Figure 2b).

Markers for As toxicity (Isayenko & Maathuis, 2008; Lindsay & Maathuis, 2017; Remy et al., 2012; Song et al., 2010) such as the phosphate transporter *AtPHT1;9*, boric acid transporter of the aquaporin family (*AtNIP7;1*), and the multidrug resistance protein *AtABCC1* showed a trend towards increased expression in roots of As-treated plants and also under Hpx and under combined stresses (Figure 2c). Apart from *ABCC1*, these marker transcripts showed no significant changes in leaves (Figure 2d).

### 3.3 | Root transcript profiles reveal stress-specific expression pattern

Root transcriptome profiles were established for each of the stresses. Stress-dependent increases in amounts greater than twofold were seen for 1,088 transcripts in As, 966 in Hpx, and 1,307 in HpxAs (Figure 3a). The overlap is shown in Venn diagrams and comprised

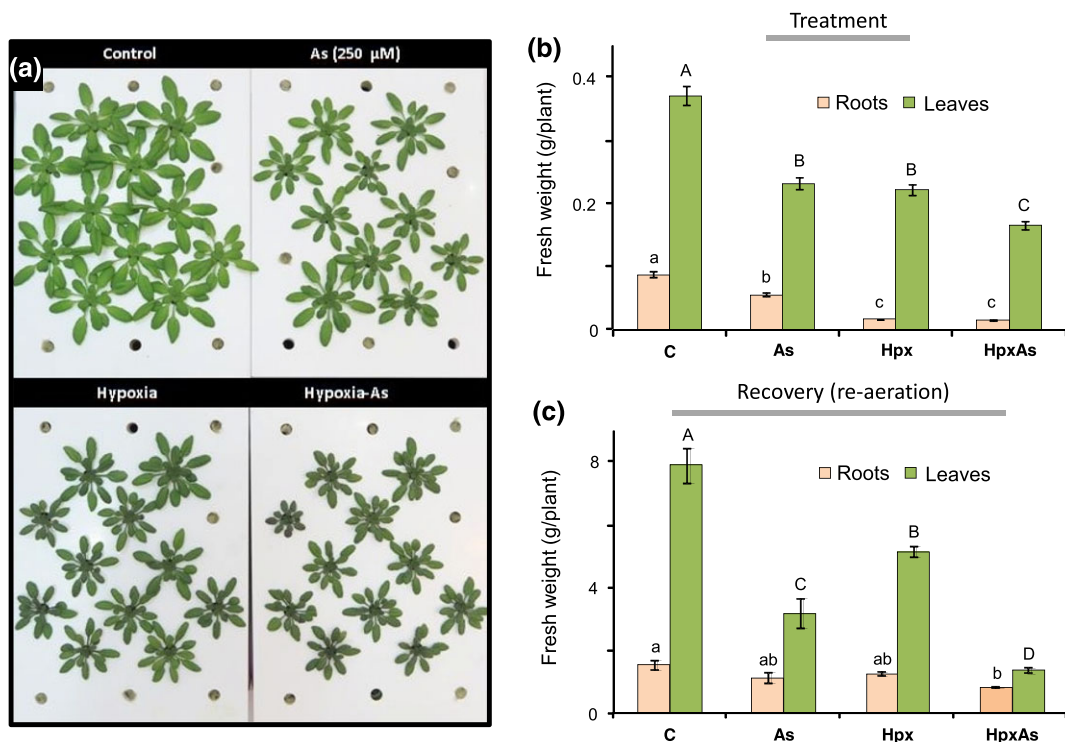


**FIGURE 1** Growth of plant exposed to arsenic (As), hypoxia (Hpx), or combined (HpxAs) stresses and subsequent recovery after re-aeration. Plants were treated with As (250  $\mu$ M), Hpx, or the combination of both stresses (HpxAs) for 7 days. For Hpx, the hydroponic medium was flushed with  $N_2$  containing 0.4%  $O_2$ . After 7 days of stress application, Hpx plants were re-aerated and recovery of plant growth was observed. (a) Plant growth phenotype as documented after 7 days of treatment. (b) Root and leaf fresh weight after 7 days of stress ( $M \pm SE$ ,  $n > 40$ ; three independent experiments). (c) The root and leaf fresh weight after 21 days of re-aeration ( $M \pm SE$ ,  $n = 12$ ). Significantly different results are labelled with different letters (one-way analysis of variance followed by Tukey's test,  $p < 0.05$ ) [Colour figure can be viewed at [wileyonlinelibrary.com](http://wileyonlinelibrary.com)]

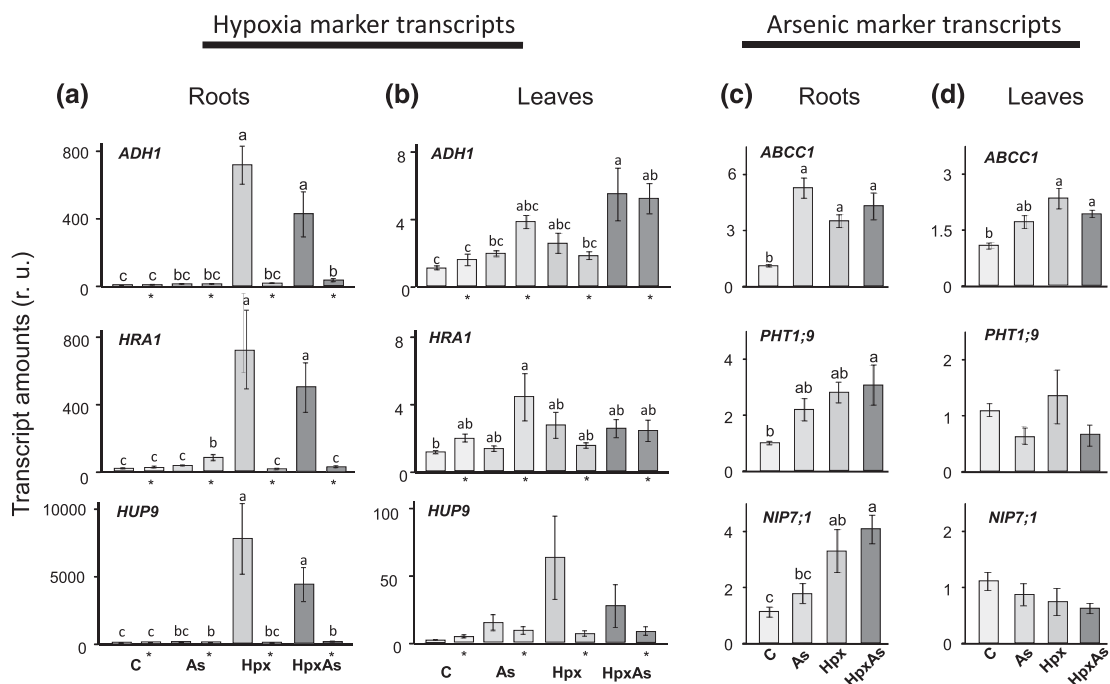


**FIGURE 2** Marker transcript analysis under arsenic (As), hypoxia (Hpx), and HpxAs stresses and subsequent recovery. Transcript amounts of Hpx (a, b) and As marker genes (c, d) after 7 days of treatment and subsequent recovery of hypoxia marker genes after 4 hr of re-aeration were analysed in roots (a, c) and leaves (b, d) by qRT-PCR. Bars marked with an asterisk are from re-aerated plants in case of hypoxia and corresponding samples for C and As. The relative change for each treatment is calculated by comparison with expression in control plants before re-aeration ( $M \pm SE$ ,  $n = 6$ ; three experiments; Tukey's test,  $p < 0.05$ ). Different letters represent significantly different means

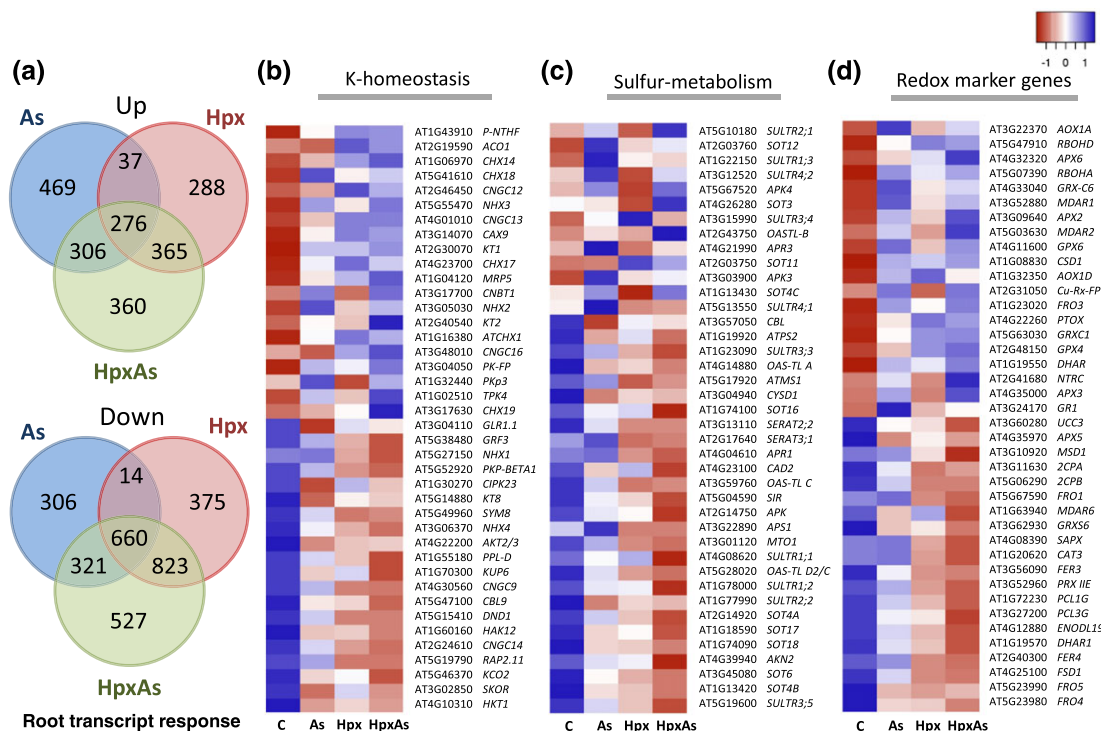


**FIGURE 3** Venn diagrams of transcripts responding to arsenic (As), hypoxia (Hpx), and HpxAs and heat maps depicting changes in transcript amounts linked to K homeostasis, S metabolism, and redox markers. (a) The diagrams depict transcripts with increased or decreased abundance in roots after 7 days of stress. Overlapping areas indicate coregulation. The stimulation or inhibition in transcript expression was calculated by comparison with control roots. Statistically significant changes are presented with thresholds of  $>2$  (increase) and less than  $-2$  (decrease;  $p < 0.05$ ,  $n = 3$ , three experiments). (b, c, d) Absolute  $\text{Log}_2$  scale values for transcript abundance under all experimental conditions were used to generate heat maps for K (b) and S homeostasis and S transport-related genes (c), and redox marker genes (d) using “HeatMapper” (<http://www.heatmapper.ca/>). The expression values are means from three independent experiments ( $p < 0.05$ ). Each map consists of the 20 most strongly increased and decreased transcripts (except for S-related transcripts with only 12 increased transcripts; Table S4) filtered as per their response to HpxAs stress. The range of expression is colour coded and ranges from red to blue, as given in scale, with red depicting the least expression

about one third of the changing transcripts with 313 transcripts common between As and Hpx; 360 transcripts were above the threshold only in the combined stress sample. Higher numbers of transcripts were seen in the sets with decreased abundance; 1,301 transcripts were down in As-treated plants, 1,872 in Hpx, and 2,331 in the combined stresses with an overlap of 674 between As and Hpx. Also important are 527 transcripts that were specifically inhibited in expression by HpxAs. Lists of the 50 most strongly responding transcripts are available in Tables S5–S9.

GO terms related to cell proliferation, rRNA metabolic process, and response to stress were overrepresented in the set with increased expression, and glucuronoxylan biosynthesis, pectin metabolic processes, cell wall synthesis, and response to osmotic stress in the set with decreased expression (Figure S1). The detailed results can be seen in Tables S2 and S3. Further, mapping of HpxAs-specific transcripts into different metabolism and transport categories is available in Figures S2 and S3. The overview of altered transcripts of metabolism revealed profound changes in cell wall and lipid metabolism (Figure S2). Here, HpxAs-specific responses of the secondary metabolic pathway transcripts are visible. Furthermore, it was apparent that transporters involved in potassium and cation transport and of the ABC type were most responsive, whereas amino acid metabolism-related transcripts showed stronger decrease (Figure S3).

We selected redox-, sulphur-, and potassium-related transcripts for a deeper dissection of the transcriptional changes (Table S4; Figure 3b–d). Potassium homeostasis genes were selected according to the report by Shabala and Cuin (2008), and the changes in transcript levels were presented as heat diagram (Figure 3a). A rather homogeneous response was seen for the  $\text{K}^+$  homeostasis-related transcripts. Highly expressed transcripts were progressively decreased under As, Hpx, and, in many cases, HpxAs stress, whereas transcripts of low abundance under control conditions accumulated under the stresses. The response of the outward-rectifying  $\text{K}^+$ -channel *SKOR* was confirmed by qRT-PCR with 40% down-regulation under Hpx and close to 90% down-regulation under As and HpxAs treatment (Figure S4).

A large set of transcripts coding for sulphur transporters and components of sulphur metabolism changed their abundance in response to the stress treatments. The low-affinity sulphate transporter *SULT3;5* and the flavonoid glycoside 7-sulphotransferase *SOT4B* were examples for transcripts with lower abundance under stresses. This was confirmed by qRT-PCR for *SOT4B* but remained statistically insignificant for *SULT3;5*. Another set showed increase under As stress and little response to Hpx. This type of response was validated for *SULT2;1* by qRT-PCR (Figure S4).

The category “redox” was based on the list of redox network genes published by Mittler et al. (2004; Figure 3c). A set of transcripts

with low abundance in control plants increased under stress, but less homogenous than in the case of potassium homeostasis. Thus, about half of the transcripts were maximally expressed in As-exposed plants, slightly less under Hpx, and the least under HpxAs. The response was validated by qPCR for *alternative oxidase 1A* (AOX1A) and the *respiratory burst oxidase homolog protein D* (RBOHD; Figure S4). Other transcripts expressed at high levels under control conditions progressively decreased with stress in the order As < Hpx < HpxAs. The change in *ferric reduction oxidase* (FRO4) expression was exemplarily confirmed by qRT-PCR (Figure S4).

### 3.4 | Severe decline in potassium contents

Deregulation of nutrient, in particular potassium homeostasis-related transcript, prompted us to analyse mineral nutrient composition in roots and rosettes (Figure 4). Arsenic contents were high in As-exposed roots and also increased in rosettes as expected. Arsenic incorporation in roots was 1.65-fold higher in As-treated roots compared with HpxAs roots. Pronounced decrease in dry weight-related potassium contents was evident in both roots and leaves of all stressed plants. Calculation of whole plant potassium contents revealed the strong decline in total potassium incorporation from 1.65 mg in control plants to 0.98 mg in As, 0.64 mg in Hpx, and 0.4 mg in combined stresses (Figure S5). Also, low in leaves were Ca, Mg, and P amounts under Hpx, whereas sulphur was high in leaves of As-treated plants.

### 3.5 | Content and state of redox metabolites

The altered transcript amounts related to redox homeostasis and the previous reports that had established a strong influence of As or Hpx stress on cell redox state prompted us to determine redox metabolites and the root cell redox state as parameters possibly influencing plant development in our experimental setup. Typical for As exposure was the up-regulation of GSH and nonprotein thiols in roots and shoots (Figure 5a,b). The high level of nonprotein thiols in As-exposed roots indicates the synthesis of PCs. Estimated PC synthesis was only half in HpxAs compared with As, correlating with the amount of incorporated As (Figure 5). Importantly, the GSH pool declined to half of control in HpxAs treatment. Leaf ascorbate amounts increased from control conditions to As exposure, Hpx, and combined stresses; thus, ascorbate was three times elevated in HpxAs compared with control (Figure 5a). H<sub>2</sub>O<sub>2</sub> dropped from the level in control roots to very low amounts in As-treated roots (Figure 5b). H<sub>2</sub>O<sub>2</sub> levels in hypoxic roots were similar to those in control roots and slightly decreased in roots exposed to combined stresses (HpxAs). In a converse manner, the leaf H<sub>2</sub>O<sub>2</sub> amounts were elevated in plants exposed to Hpx in the rooting medium.

The amount and redox state of the mitochondrial peroxiredoxin PrxIIIF was exemplarily explored in root and leaf extracts of differently treated plants (Figure 5a). No differences in PrxIIIF amounts were discernible between the treatments in both roots and leaves. Leaf and root proteins were also extracted in buffer containing mPEG<sub>5000</sub>-maleimide to label reduced thiols. The majority of PrxIIIF was present in the oxidized form running as lower band. The reduced fraction was small in

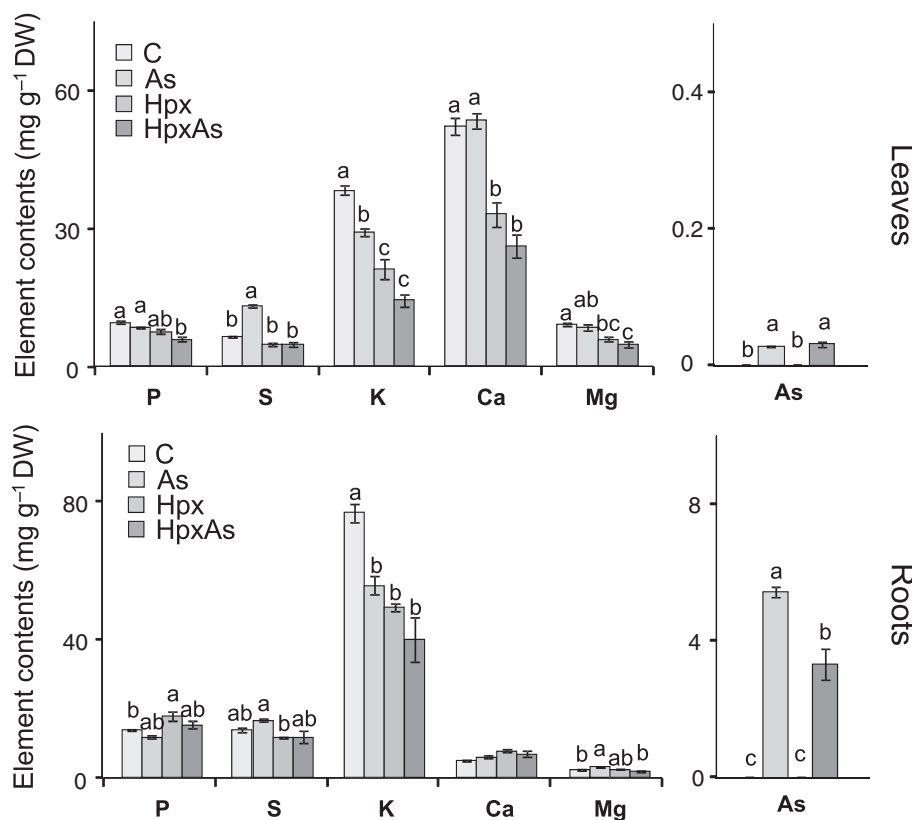


**FIGURE 4** Elemental analyses in arsenic- (As), hypoxia- (Hpx), and HpxAs-treated *Arabidopsis thaliana*. Arsenic and macroelements were quantified after 7 days of stress. Data are presented as  $M \pm SE$ ,  $n = 4$  experiments (Tukey's test,  $p < 0.05$ ). Different letters label significantly different means for individual elements (the relative water content and total K per plant are given in Figure S5)



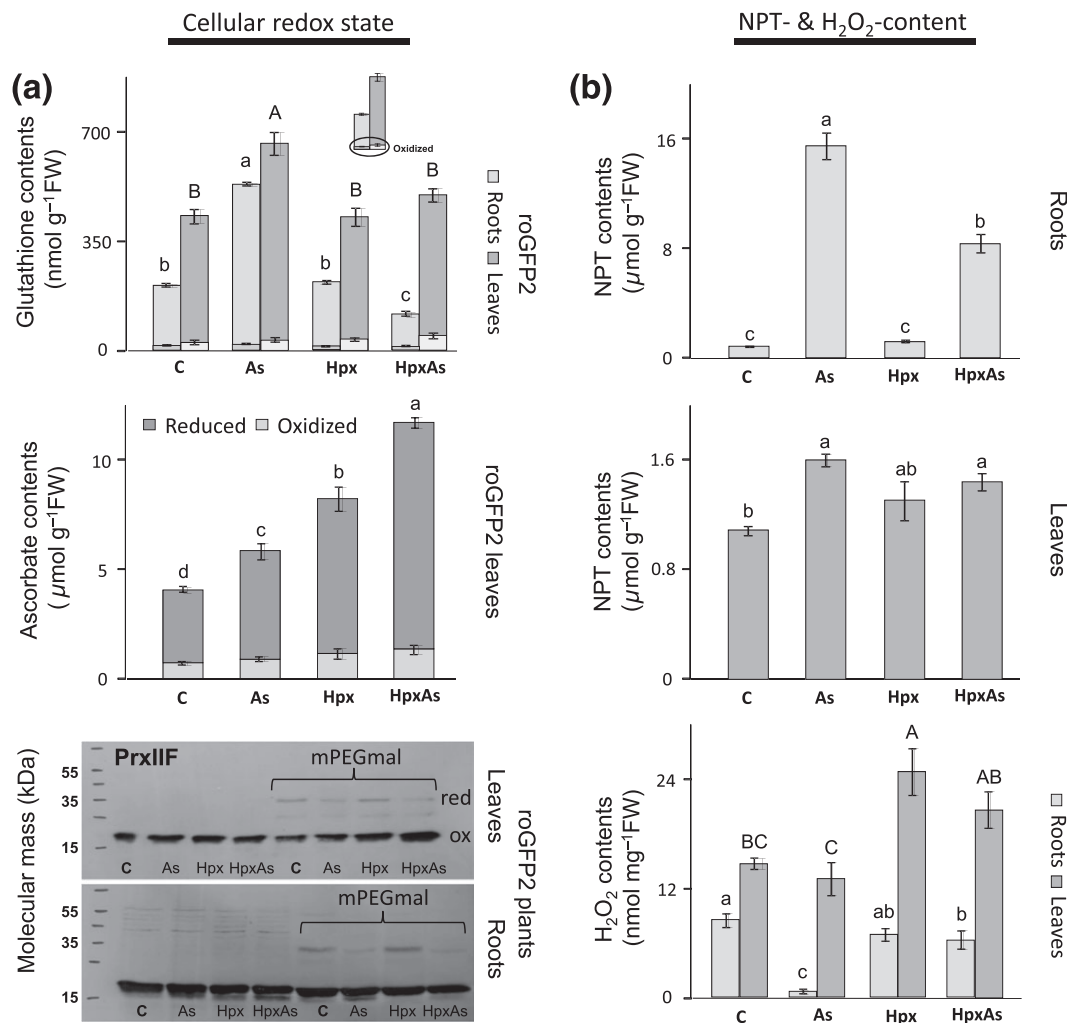


**FIGURE 5** Redox metabolites and nonprotein thiols. (a) Contents and redox status of glutathione were measured in leaves and roots of roGFP2 plants (Grx1-roGFP2) treated with arsenic (As), hypoxia (Hpx), or HpxAs for 7 days. Oxidized and reduced ascorbate contents were analysed in leaves of these plants but were undetectable in roots. Redox status of mitochondrial peroxiredoxin IIF (PrxIIIF) was analysed in differentially treated plants. Protein extraction in presence of methoxypolyethylene glycol maleimide (mPEGmal) labelled the sulphhydryl groups. Immunoblotting was performed using PrxIIIF specific antibodies after separating proteins of three experiments. (b) Nonprotein thiols (NPTs) and H<sub>2</sub>O<sub>2</sub> contents were measured in leaves and roots of *Arabidopsis thaliana* (Col-0) after 7 days of treatment. Data are  $M \pm SE$ ,  $n = 9$  (NPTs and H<sub>2</sub>O<sub>2</sub>; three experiments) and  $n = 10$ – $12$  (glutathione and ascorbate; four experiments). Different capital (leaves) or lower-case letters (roots) indicate significance of difference (Tukey's test;  $p < 0.05$ )

the control and Hpx samples and further decreased in As and combined stresses. Similar patterns were observed for roots and leaves (Figure 5a).

### 3.6 | Effect on the cytosolic GSH redox state

The changed redox parameters prompted us to estimate the cytosolic GSH redox state in vivo using the redox-sensitive reporter roGFP2 fused to glutaredoxin and stably expressed in *A. thaliana*. The fluorescence ratio at 405 to 488 nm allows calculating the  $E_{GSH}$ . It should be noted that this calculation at low 405/488 ratios only gives an estimate because the probe saturates. Thus, the given redox potentials should be considered with care below  $-315$  mV. The redox potential shifted from highly negative values to more positive values in As-treated roots within 60 min (Figure 6a). This shift was also seen in the combined stresses, whereas  $E_{GSH}$  initially remained unchanged in hypoxic roots and only increased afterwards. The changes in cytosolic  $E_{GSH}$  were further manifested during the subsequent 7-day treatment period (Figure 6b). The

highest value in As-treated roots was detected after 2–4 days. Subsequently, the redox potential reversed to more negative values, whereas it increased further in the combined stresses. The micrographs of root tips (Figure 6c) exemplarily depict the raw data for ratiometrically determined readouts of the redox potentials after 7 days of treatment. The shift to oxidizing conditions was observed in the cell layers underneath the rhizodermis and also covered the area of the quiescent centre and the descendant cell arrays. The shift was strong in arsenic-treated roots and particularly pronounced in roots exposed to combined stresses.

### 3.7 | Stress-dependent hormone levels in leaves and roots

The redox and nutrient imbalance and the altered growth pattern were expected to interfere with the hormonal state of the plants and vice versa. The increased shoot-to-root fresh weight ratio (Figure S5a) likely compromised the water status as reflected by increased abscisic acid

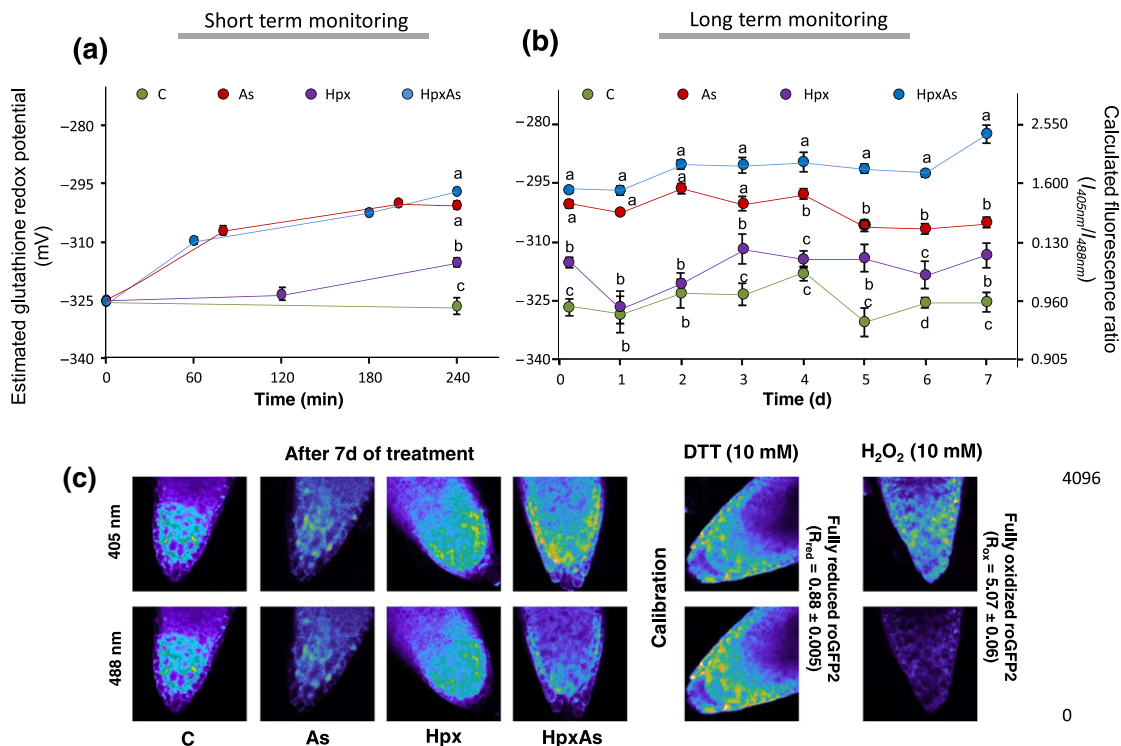


**FIGURE 6** Ratiometric analysis of glutathione redox potential in root cells. The in vivo redox state of the cytosolic glutathione pool was analysed in root cells of arsenic- (As), hypoxia- (Hpx), and HpxAs-treated roGFP2-expressing plants. Roots were illuminated with 405 and 488 nm, and the roGFP2 fluorescence was recorded. The fluorescence ratio was used to calculate the redox state of roGFP2 corresponding to the estimated cytosolic glutathione redox potential (left y-axis; on the second y-axis in [b] the ratios  $I_{405nm}/I_{488nm}$ ). The calculation of redox potential was based on calibration, where complete reduction and oxidation of roGFP2 were achieved with 10 mM DTT or  $H_2O_2$ , using the Nernst equation. The calculated average  $I_{488ox}/I_{488red}$  was  $0.26 \pm 0.014$  for  $n = 25$  independent calibration sets. Average values of  $R_{red}$  and  $R_{ox}$  were calculated from  $n = 252$  and  $243$  independent root tips, respectively, and are exemplarily presented in (c). Roots of stressed plants were analysed from 0 to 4 hr (a) and from Day 0 to Day 7 (b) of start of treatment, and data represent  $M \pm SE$ ,  $n = 12-20$ , from two experiments (two-way analysis of variance with post hoc Tukey's test,  $p < 0.05$ ). Significance of difference was calculated for each day and was marked by different letters. (c) The micrographs present representative images recorded at 405 and 488 nm after 7 days of treatment. Also shown are representative images obtained after treatment with 10 mM  $H_2O_2$  for full oxidation and 10 mM DTT for full reduction [Colour figure can be viewed at [wileyonlinelibrary.com](http://wileyonlinelibrary.com)]

levels in stressed rosettes (Figure 7). Variation of hormone levels between the four independent experiments was very high. Thus, despite large changes of mean values, significance was only revealed for a few hormones and conditions. Oxophytodienoic acid (OPDA) functions as precursor of jasmonic acid (JA) but also exerts JA-independent roles (Maynard, Gröger, Dierks, & Dietz, 2018). OPDA was tentatively increased in rosettes under As and Hpx and was particularly strong in the combined stress treatment. OPDA was decreased in stressed roots. To elucidate the hormonal state with additional parameters, selected marker transcripts were quantified in roots of treated plants. Transcript levels of the sulphurase (ABA3) and the protein kinase OST1 increased in roots with higher ABA contents in leaves. Both marker transcripts accumulated in the stress treatments, particularly OST1, which increased in the order of As < Hpx < HpxAs treatment. The JA marker transcripts *SRG2* and *lipoxigenase LOX1* were elevated under stress in roots; however, JA contents were invariable among different treatments and showed no significant change in roots or shoot.

### 3.8 | Photosynthetic performance

Parameters of photosynthesis, pigments, and kinetic parameters were determined in order to assess the effects on leaf metabolism

of the stressors, which primarily act on roots. Anthocyanins strongly accumulated in plant exposed to Hpx or combined stresses (Figure 8c), whereas photosynthesis-related parameters were not significantly different between the treatments (Figure 8a). Only very early after 4 hr of treatment were kinetic parameters distinctly changed in a short illumination experiment (Figure 8b). The Fdx pool was most reduced upon illumination in leaves of those plants that were exposed to Hpx and the least in As-treated plants. Interestingly, the redox kinetics of Fdx under combined stresses deviated the least among all treatments from control conditions (Figure 8b).

Lack of  $O_2$  inhibits the respiratory electron transport, the citric acid cycle, and efficient ATP production. In this metabolic context, it appeared interesting to quantify soluble and nonsoluble sugars as indicators of the metabolic state (Figure S6). Both soluble and nonsoluble sugars, which mostly represent starch, significantly increased in leaves of hypoxic plants and also in plants exposed to combined As and Hpx stresses. Soluble sugar contents were slightly elevated in roots from stressed plants, as were the insoluble sugars in Hpx- and HpxAs-treated plants. Thus, carbohydrate availability was ample and unlikely limited growth under stress.

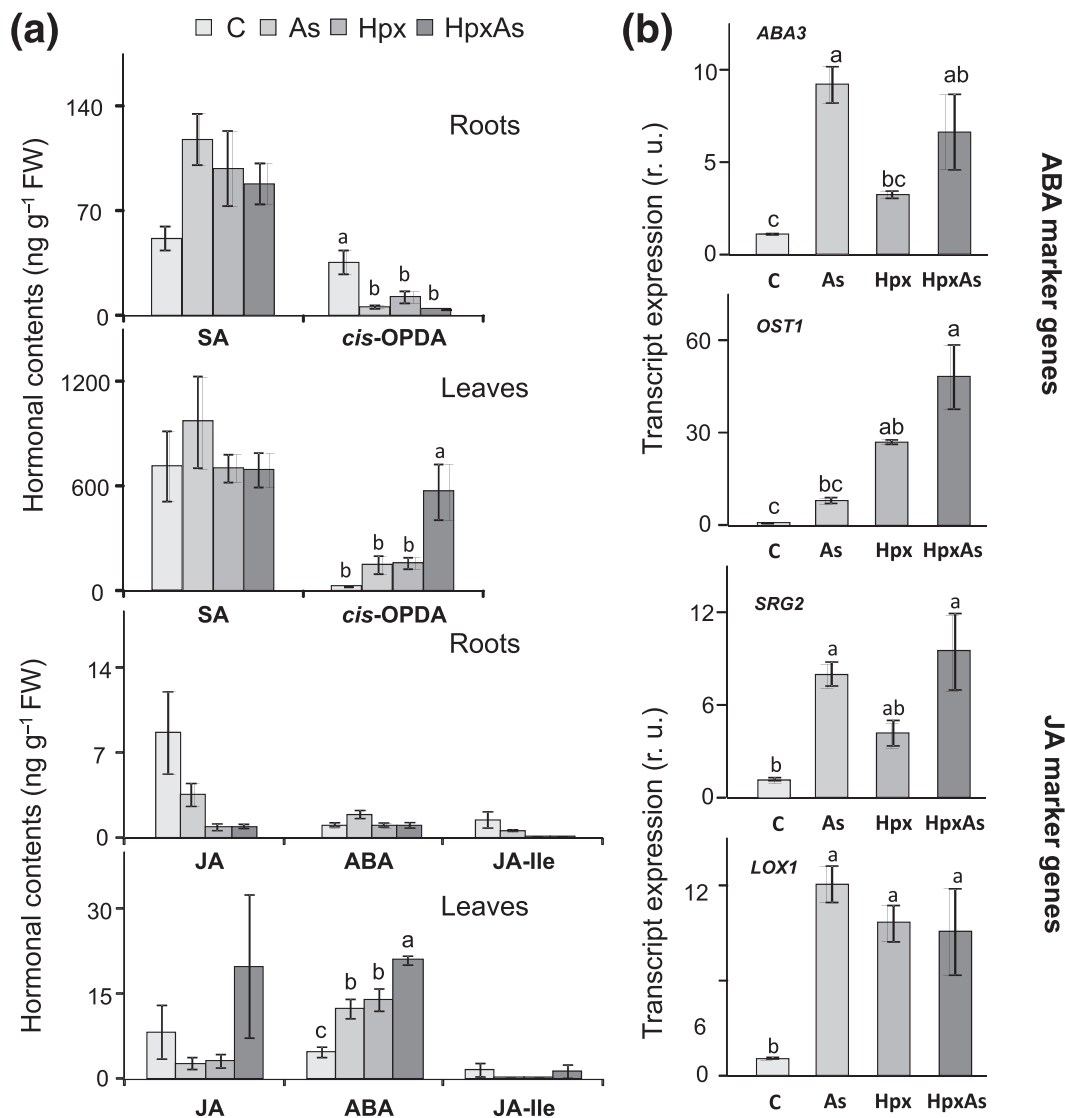


**FIGURE 7** Hormone levels in leaves and roots and abundance of selected hormone marker transcripts in roots of arsenic (As), hypoxia- (Hpx), and HpxAs-treated plants. (a) Hormone levels in leaves and roots at Day 7 ( $M \pm SE$ ,  $n = 4$ ; four experiments; Tukey's test,  $p < 0.05$ ). Different letters indicate groups of significant difference. (b) Relative marker transcript amounts for abscisic acid (ABA) and jasmonic acid (JA) as analysed in roots of stressed plants by qRT-PCR. Data are  $M \pm SE$ ,  $n = 4$  (two experiments; Tukey's test,  $p < 0.05$ ). Different letters signify significantly different means

## 4 | DISCUSSION

### 4.1 | Establishment of Hpx for roots and normoxia for leaves

To approach the response of *A. thaliana* to Hpx and arsenic as combinatorial stresses, it was important to choose appropriate conditions that resemble natural stress levels. The aeration of the hydroponics medium with normal air (21% O<sub>2</sub>) as control or air with 0.4% O<sub>2</sub> as hypoxic treatment established severe but reversible Hpx stress as shown by efficient resumption of root growth after reoxygenation (Figure 1). Decreasing amounts of Hpx marker transcripts showed the rapid initiation of transcript degradation upon resumption of normoxia (Figure 2). This response also involves degradation of transcription factors, for example, with the N-end rule mechanism (Gibbs et al., 2011; Licausi et al., 2011; Sasidharan & Mustroph, 2011). The recovery was slightly compromised by the presence of As for some transcripts (Figure 2). Interestingly, the normoxic leaves also rapidly

perceived the stress state of the roots. The leaves initiated acclimation events leading to adjustment of photosynthesis and assimilate partitioning (Figure 8; Figure S6). Neither roots nor leaves were deficient in carbohydrates.

The results from the transcript analysis in roots demonstrated the peculiarities and similarities of the single and combined treatments (Figure 3, Figures S1–S4). A set of 887 genes responded specifically to the combined stress treatment, the bigger portion (527) of which was down-regulated (Figure 3). The biochemical and transcriptome data obtained in this study will be discussed with respect to the local stress response and long-distance effects in the following account.

### 4.2 | Local effects of arsenic, Hpx, and combined stresses in roots

#### 4.2.1 | Cytosolic redox state

The cytoplasmic redox potential of root cells strongly increased within a few hours upon addition of As and HpxAs; the increase was slightly

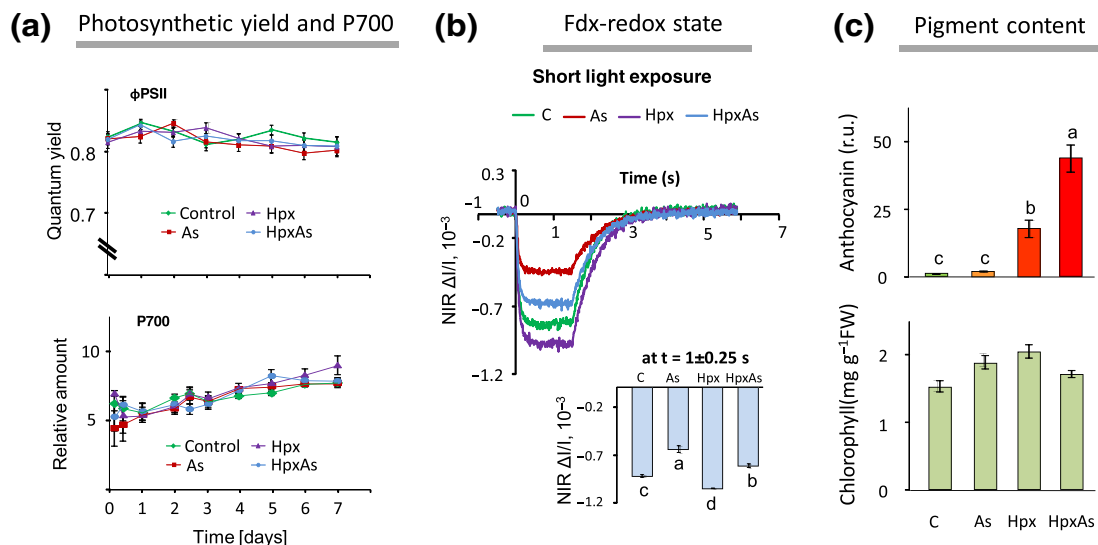


**FIGURE 8** Photosynthesis-related parameters and pigment contents. (a) Stress effects on the photosynthetic quantum yield ( $\Phi$ PSII) and photosystem amount (P700) as measured at specific time points. Data are  $M \pm SE$ ,  $n = 60$  ( $\Phi$ PSII; three experiments),  $n = 2-6$  (P700; three experiments except at 4 and 8 hr where data are from two experiments). (b) Effect of As, hypoxia, and HpxAs on kinetic change of ferredoxin (Fdx) redox state upon exposure to a short (1.5-s) pulse of light ( $160 \mu\text{mol quanta m}^{-2} \text{s}^{-1}$ ) in dark-adapted leaves of *Arabidopsis thaliana* (Col-0) 4 hr after start of stress application. Data represent  $M \pm SE$ ,  $n = 4$  (two independent experiments). Statistical analysis (one-way analysis of variance) for differences among means was performed at  $t = 1 \pm 0.25$  s. Different letters represent significantly different means (Tukey's test;  $p < 0.05$ ). (c) Anthocyanin and chlorophyll contents as measured after 7 days of treatment ( $M \pm SE$ ,  $n = 9$ ; three experiments; Tukey's test,  $p < 0.05$ ). Different letters give significantly different means [Colour figure can be viewed at [wileyonlinelibrary.com](http://wileyonlinelibrary.com)]

delayed and of lower magnitude in Hpx (Figure 5). The likely reason is the decrease in cell energization (ATP/ADP) by inhibition of mitochondrial respiration and disturbance of mitochondrial redox homeostasis in the presence of As (Chen et al., 2014). The partial recovery of the cytosolic redox potential under As during the prolonged 7-day exposure indicates acclimation presumably by vacuolar compartmentation mediated by ABCC1 and ABCC2 (Sharma, Dietz, & Mimura, 2016; Song et al., 2010). However, the deviation from redox homeostasis was still enhanced in the combined stresses despite the lower accumulation of As (Figure 6). This may be attributed to inefficient As sequestration under HpxAs stress, compared with single As stress, due to inadequate PC synthesis as a consequence of lower sulphur and GSH amounts (Figures 4 and 5). Further, the incomplete relief from Hpx under As stress might be due to the ongoing growth in the presence of As stress only. The increase in biomass may assist in removing As from the root tip cells by As distribution in a larger tissue volume. In a converse manner, the ceased root growth in HpxAs impeded dilution of As by biomass increase (Figure 1).

The long-term readjustment of the cytosolic redox potential in As-treated roots (Figure 6b) might be explained by de novo synthesis induced by the changed GSH/GSSG ratio (Noctor et al., 2012). Interestingly, up-regulation of the vacuolar As transporter ABCC1 also occurred under Hpx and HpxAs, suggesting some redox-dependent effects on gene expression (Figure 2).

The results from redox imaging in the root tip only partly matched the response of the GSH pool measured in whole root extracts (Figure 5). Apparently, the root tip including the calyptra, the quiescent centre, and the descendant cells are particularly sensitive targets of Hpx and As stresses (Dho, Camusso, Mucciarelli, & Fusconi, 2010), whereas the older plant tissues that dominate the result from total

root analysis were less affected by single As stress but severely affected in the combined stresses. Thus, the GSH and the nonprotein thiol pools were increased in roots under As stress, remained unchanged in Hpx, but decreased in HpxAs. Efficient synthesis of thiol compounds plays a central role in realizing As tolerance. A major portion of the cellular sulphur in the presence of As is drained into PC synthesis (Schmöger et al., 2000).

Increased sulphur availability and thereby altered S metabolism improve performance of rice upon As stress (Dixit et al., 2015). The transcript of the plastid O-acetylserine(thiol)lyase OASTL-B was strongly increased in HpxAs roots (Figure 3). This may indicate the activation of a regulatory feedback to restore the GSH pool in the roots. However, the up-regulation of transcripts was insufficient as revealed by the low GSH pool in roots of HpxAs plants (Figure 5). It is concluded that the altered redox potential and the lowered GSH amounts likely contribute to the growth arrest of plants exposed to HpxAs (Vernoux et al., 2000). Nonprotein thiol accumulation (PCs) correlated with As-amounts, that is, with efficient As sequestration in roots and very small amounts detected in leaves.

#### 4.2.2 | Sulphur homeostasis and metabolism

The interference of Hpx, As, and combined stresses with S metabolism is also apparent from the transcriptome analysis (Figure 3). Transcript accumulation of most sulphate transporters was altered often under all three stress conditions (Figure 3). Expression of the vacuolar *SULTR4;2* was stimulated by As but not affected by the combined stresses. *SULTR4;2* controls the efflux of vacuolar sulphate into the cytosol to optimize the internal sulphur distribution under sulphur deprivation (Kataoka et al., 2004; Zuber et al., 2010).



Transcript of *SULTR2;1*, which mediates transfer of sulphate from old to young leaves (Kataoka, Hayashi, Yamaya, & Takahashi, 2004), accumulated in HpxAs, whereas transcript of *SULT3;5*, which transports sulphate from the root to the shoot, decreased under all stress conditions (Figure 3). Transcript amounts of high-affinity sulphate transporters *SULTR1;1* and *SULTR1;2* (El-Zohri, Odjegba, Ma, & Rathinasabapathi, 2015) strongly decreased in the HpxAs treatment (Figure 3). These two genes influence As accumulation in roots and induce its translocation to the shoot but do not inhibit As uptake. Interestingly, along with decreased As accumulation in roots, phosphate accumulation and potassium accumulation are also impeded (El-Zohri et al., 2015). A similar pattern was observed under HpxAs for root P and K contents along with lower As accumulation (Figure 4).

#### 4.2.3 | Redox and ROS homeostasis transcripts

The change in redox state was reflected in altered accumulation of redox-related transcripts (Figure 3, Figure S2). Amounts of many iron homeostasis- and antioxidant defence-related transcripts were low under the stress treatments, particularly under HpxAs (Figure 3). This group includes *peroxiredoxin IIE* with a role in chloroplast stress defence (Romero-Puertas et al., 2007), *monodehydroascorbate reductase 6 (MDAR6)*, and cytosolic *dehydroascorbate reductase 1 (DHAR1)* with roles in stress defence against toxins, GSH oxidation, and salicylic acid signalling (Johnston et al., 2015; Rahantaniaina et al., 2017) and *catalase 3* (Tiew, Sheahan, & Rose, 2015). CAT3 function has been linked to cell division because *cat3*-mutants were compromised in cell division induction (Tiew et al., 2015).

Transcript amounts coding for *AOX1A* were strongly increased under As, whereas *AOX1D* was up under Hpx. The response was smaller in the combined stresses. AOXs play important roles in fine-tuning the mitochondrial respiratory activity and the cellular redox state particularly under stress (Saisho et al., 1997; Selinski et al., 2018). Such a contrasting response was seen for several redox-related transcripts. Like *AOX1A*, transcripts coding for *glutathione reductase 1* and *glutaredoxin C6* were strongly induced in As but scarcely responded in Hpx and HpxAs (Figure 3).

The simultaneous exposure to As and Hpx aggravated the experienced stress. This is evident from the delayed recovery of HpxAs plants after 7 days of stress. The root growth of HpxAs plants, compared with the control, remained slow after reaeration, whereas root growth of As- and Hpx-stressed plants caught up with that of the control (Figure 1). Apparently, the plants encounter cumulative effects that establish long-lasting physiological modifications and inhibit resumption of growth. Such enduring stress effects could involve GSH-dependent processes (Diaz Vivancos, Wolff, Markovic, Pallardó, & Foyer, 2010), which also affect epigenetic processes. Notably, the persistent stress effects were not related to excessive As accumulation because on a dry-weight basis As accumulated less in HpxAs than in As (Figure 4).

#### 4.3 | Stress signalling and photosynthesis

The establishment of Hpx in the rooting medium caused rapid changes in the rosettes and leaf metabolism (Figures 1 and 8). It is concluded that long-distance effects link the metabolic state of the roots to that of the shoot. Candidate information mechanisms concern a backlog of

assimilates (Figure S6) due to decreased assimilate consumption in the roots and thus inhibited sink activity, lack of nutrients (Figure 4) due to inhibited uptake in the roots, redox signals (Figure 5), and hormones (Figure 7; see also Jackson, 2002).

Within a few hours, the photosynthetic machinery adopted a different state in the differently exposed plants. Most pronounced were the differences in Fdx levels, namely, strongly lowered Fdx reduction in As-exposed plants and increased Fdx reduction in Hpx-treated plants (Figure 8). Fdx functions as a hub in electron distribution downstream of PSI. Its increased reduction may indicate decreased drainage of electrons by reductive metabolism in leaves under Hpx as long as the metabolic adjustment has not been optimized (Bukhov & Carpentier, 2004). In a converse manner, As stress may transiently increase the demand for reductive power because arsenic functions as an uncoupling agent (Good, 1977). The combined exposure to Hpx and As mediated an intermediate Fdx redox state.

The increase in anthocyanin contents along with the accumulation of the redox metabolite ascorbate in leaves of Hpx- and HpxAs-treated plants (Figures 5 and 8) may protect the leaf cells from oxidative damage (Das & Roychoudhury, 2014; Foyer & Noctor, 2012).

The shift towards a more oxidized state of the cytosol and mitochondria in roots was evident from the  $H_2O_2$  accumulation and decreased reduction of PRXIIIF in HpxAs-treated plants (Figure 5). The As response was different because root growth was maintained albeit with lower rate leading to a proportional decrease of both root and shoot growth (Figure 1).

The differences in photosynthetic state were compensated within less than 2 days showing the efficient adjustment of the photosynthetic apparatus despite the severe drop in assimilate demand in Hpx and HpxAs (Figure 1). The adjustments of the photosynthetic apparatus coincided with anthocyanin accumulation on the abaxial side of the leaf. Anthocyanin accumulation is an established indicator for metabolic changes and plays an adaptive role under stress. With longer stress impact, all measured photosynthetic parameters were indistinguishable between the treatments, that is,  $\Phi$ PSII and PSI redox state (Figure 8), whereas sugars and starch accumulated (Figure S6).

#### 4.4 | A role for hormones in signalling under combined stresses

Here, the well-aerated leaves of the plants under Hpx and combined stresses showed hyponasty, a well-documented Hpx response (Colmer & Voesenek, 2009). The involved signalling pathways were proposed to be carbohydrate independent (Jackson, 2002). It is known for free ABA and ABA conjugates to act as a long-distance signal (Sauter, Dietz, & Hartung, 2002). Leaf water status changed in Hpx- and HpxAs-treated plants (Figure S5) and is evident from the strong accumulation of transcripts of *OST1*, the core ABA signalling component that responds to leaf water status (Susmilch, Atallah, Brodribb, Banks, & McAdam, 2017; Figure 7). Further, the highly increased shoot-to-root ratio is a rather peculiar response brought about by the strong Hpx-induced inhibition of root growth (Figure 1). Stresses like salinity and drought induce contrasting responses, namely, shoot growth inhibition and root growth stimulation to minimize aerial water loss, and increase the nutrient and water uptake by the roots as, for example,

shown for tomato (Albacete et al., 2008). Because Hpx involves ethylene as signalling molecule that mediates growth inhibition, it is interesting that ABA exerts an antagonizing role that may decrease the ethylene-dependent inhibition (Sharp & LeNoble, 2002). Thus, it might be speculated that ABA accumulation in the shoots might play a role in maintaining shoot growth under Hpx and HpxAs.

*cis*-OPDA accumulated strongly in leaves, especially under combined stress treatment. Unlike ABA, *cis*-OPDA is synthesized in the chloroplasts under stress. *cis*-OPDA functions as precursor of JA synthesis but also acts as a JA and *COI1*-independent signalling compound, both triggering acclimation responses to stress (Maynard et al., 2018; Okazaki & Saito, 2014; Wasternack & Strnad, 2016). OPDA influences the gene expression of redox metabolism-related genes like *OXI1*, essentially linked to oxidative burst signal transduction pathway in *Arabidopsis* (Taki et al., 2005). Further, it should be noted that regulation of S metabolism was recently linked to OPDA by stimulating cysteine synthesis (Park et al., 2013). Also, as a signalling molecule independent of JA and its derivatives, OPDA has been implicated to interact with ABA and in turn regulates seed germination in *A. thaliana* (Dave & Graham, 2012). The interference of *cis*-OPDA- and ABA-dependent signalling pathways may have adaptive implications for the plants under combined stresses and should be further investigated.

#### 4.5 | Severe disturbance of potassium homeostasis

As a consequence of disproportionate inhibition of root growth and impeded root metabolism (Figure 1), uptake of several nutrients was decreased under all stress treatments. Declined shoot levels of  $K^+$ ,  $Mg^{2+}$ ,  $Ca^{2+}$ , and phosphorus indicate a severe nutritional disorder (Figure 4). The decreased  $K^+$  and  $Mg^{2+}$  uptake and translocation could restrict shoot growth under these treatments. Potassium homeostasis has been recognized as an important regulator of plant growth under Hpx. Wang et al. (2017) used mutants lacking a functional potassium channel of the GORK type and observed that the improved  $K^+$ -retention in the roots ameliorated plant performance under Hpx. The mutant realized a water logging-tolerant phenotype.

Several  $K^+$ -related transcripts that were expressed at a low level under control conditions accumulated under stress, for example, the *potassium transporter 1* and 2 (*KT1*, *KT2*), and also the *cation proton exchanger CHX14* (Figure 3). *CHX14* regulates  $K^+$  redistribution in the plant body. This could indicate the activation of mechanisms to counteract the  $K^+$  shortage. Other potassium-related transcripts that were highly expressed under control conditions were repressed under the stresses, for example, the outward-rectifying  $K^+$ -channel *SKOR* delivering  $K^+$  to the xylem (Figure 3). The profound reorganization of the potassium-related transcriptome was striking and supports the conclusion that disturbance of potassium homeostasis significantly contributes to the observed growth phenotypes.

## 5 | CONCLUSION

The presence of multiple abiotic factors above or below their optimum intensity for plant growth and development is a common phenomenon

in nature. Here, the naturally occurring combination of Hpx, for example, following flooding, and arsenic exposure was addressed and revealed responsiveness of the plant exposed to combinatorial stresses distinct from that of plants treated with Hpx or arsenic individually. The rapid (within 1 hr) changes in root cell redox potential and the redox shift (within 4 hr) of components of the photosynthetic electron transport (e.g., Fdx) indicate fast long-distance effects within the plant. Along with ROS and sugars, ABA and the JA precursor *cis*-OPDA may play crucial roles in acclimation to combined stresses. In addition to disturbance of redox homeostasis, the aggravation of nutrient disorder, in particular of K and S, under HpxAs stress is suggested to impose a severe constraint on plant performance. Following reaeration, the rapid decline in Hpx marker transcripts indicated recovery of plants from both single and combined stresses. However, the resumption of growth in HpxAs plants was compromised after reaeration pointing to persistent physiological effects and manifested damage despite lower accumulation of As. It will be important to more closely scrutinize the 360 and 527 transcripts that were specifically increased and decreased, respectively, in the combined stresses as compared with single stresses. It is hypothesized that they will provide clues on the nature of the long-lasting stress effects following HpxAs exposure.

#### ACKNOWLEDGEMENTS

A fellowship award to V. K. from DAAD, Bonn, Germany, is thankfully acknowledged. V. K. also acknowledges the financial support in the form of junior research fellowship by Indian Council of Medical Research (ICMR), New Delhi, for the PhD work in India. The expert technical assistance by Martina Holt and Heike Bogunovic and support by the Deutsche Forschungsgemeinschaft are gratefully acknowledged (K.-J. D.: SPP1710; A. J. M.: RTG2064, SPP1710, ME1567/9-1/2).

#### CONFLICT OF INTEREST

The authors did not encounter any conflict of interest.

#### ORCID

Vijay Kumar  <http://orcid.org/0000-0002-7771-4269>

Andreas Meyer  <http://orcid.org/0000-0001-8144-4364>

Stephan Clemens  <http://orcid.org/0000-0003-0570-1060>

Karl-Josef Dietz  <http://orcid.org/0000-0003-0311-2182>

#### REFERENCES

- Abercrombie, J. M., Halfhill, M. D., Ranjan, P., Rao, M. R., Saxton, A. M., Yuan, J. S., & Stewart, C. N. (2008). Transcriptional responses of *Arabidopsis thaliana* plants to As(V) stress. *BMC Plant Biology*, 8(1), 87.
- Albacete, A., Ghanem, M. E., Martínez-Andújar, C., Acosta, M., Sánchez-Bravo, J., Martínez, V., ... Pérez-Alfocea, F. (2008). Hormonal changes in relation to biomass partitioning and shoot growth impairment in salinized tomato (*Solanum lycopersicum* L.) plants. *Journal of Experimental Botany*, 59, 4119–4131.
- Aranda, P. S., LaJoie, D. M., & Jorcyk, C. L. (2012). Bleach gel: A simple agarose gel for analyzing RNA quality. *Electrophoresis*, 33(2), 366–369.
- Babicki, S., Arndt, D., Marcu, A., Liang, Y., Grant, J. R., Maciejewski, A., & Wishart, D. S. (2016). HeatMapper: Web-enabled heat mapping for all. *Nucleic Acids Research*, 44(W1), W147–W153.

- Bailey-Serres, J., & Chang, R. (2005). Sensing and signalling in response to oxygen deprivation in plants and other organisms. *Annals of Botany*, 96(4), 507–518.
- Bailey-Serres, J., & Voeselek, L. A. C. J. (2008). Flooding stress: Acclimations and genetic diversity. *Annual Review of Plant Biology*, 59, 313–339.
- Bailey-Serres, J., & Voeselek, L. A. C. J. (2010). Life in the balance: A signaling network controlling survival of flooding. *Current Opinion in Plant Biology*, 13(5), 489–494.
- Bankaji, I., Sleimi, N., López-Climent, M. F., Perez-Clemente, R. M., & Gomez-Cadenas, A. (2014). Effects of combined abiotic stresses on growth, trace element accumulation, and phytohormone regulation in two halophytic species. *Journal of Plant Growth Regulation*, 33(3), 632–643.
- Blokhina, O., & Fagerstedt, K. V. (2010). Oxidative metabolism, ROS and NO under oxygen deprivation. *Plant Physiology and Biochemistry*, 48(5), 359–373.
- Bohnert, H. J., Gong, Q., Li, P., & Ma, S. (2006). Unraveling abiotic stress tolerance mechanisms—Getting genomics going. *Current Opinion in Plant Biology*, 9(2), 180–188.
- Bradford, M. M. (1976). A rapid and sensitive method for the quantitation of microgram quantities of protein utilizing the principle of protein-dye binding. *Analytical Biochemistry*, 72(1–2), 248–254.
- Bukhov, N., & Carpentier, R. (2004). Alternative photosystem I-driven electron transport routes: Mechanisms and functions. *Photosynthesis Research*, 82, 17–33.
- Catarecha, P., Segura, M. D., Franco-Zorrilla, J. M., García-Ponce, B., Lanza, M., Solano, R., ... Leyva, A. (2007). A mutant of the *Arabidopsis* phosphate transporter PHT1; 1 displays enhanced arsenic accumulation. *The Plant Cell*, 19(3), 1123–1133.
- Chen, W., Taylor, N. L., Chi, Y., Millar, A. H., Lambers, H., & Finnegan, P. M. (2014). The metabolic acclimation of *Arabidopsis thaliana* to arsenate is sensitized by the loss of mitochondrial LIPOAMIDE DEHYDROGENASE2, a key enzyme in oxidative metabolism. *Plant, Cell & Environment*, 37, 684–695.
- Colmer, T. D., & Voeselek, L. A. C. J. (2009). Flooding tolerance: Suites of plant traits in variable environments. *Functional Plant Biology*, 36(8), 665–681.
- Das, K., & Roychoudhury, A. (2014). Reactive oxygen species (ROS) and response of antioxidants as ROS-scavengers during environmental stress in plants. *Frontiers in Environmental Science*, 2, 53.
- Dave, A., & Graham, I. A. (2012). Oxylipin signaling: A distinct role for the jasmonic acid precursor *cis*-(+)-12-oxo-phytodienoic acid (*cis*-OPDA). *Frontiers in Plant Science*, 3, 42.
- Dho, S., Camusso, W., Mucciarelli, M., & Fusconi, A. (2010). Arsenate toxicity on the apices of *Pisum sativum* L. seedling roots: Effects on mitotic activity, chromatin integrity and microtubules. *Environmental and Experimental Botany*, 69, 17–23.
- Diaz Vivancos, P., Wolff, T., Markovic, J., Pallardó, F. V., & Foyer, C. H. (2010). A nuclear glutathione cycle within the cell cycle. *Biochemical Journal*, 431, 169–178.
- Dixit, G., Singh, A. P., Kumar, A., Singh, P. K., Kumar, S., Dwivedi, S., ... Tripathi, R. D. (2015). Sulfur mediated reduction of arsenic toxicity involves efficient thiol metabolism and the antioxidant defense system in rice. *Journal of Hazardous Materials*, 298, 241–251.
- El-Zohri, M., Odjegba, V., Ma, L., & Rathinasabapathi, B. (2015). Sulfate influx transporters in *Arabidopsis thaliana* are not involved in arsenate uptake but critical for tissue nutrient status and arsenate tolerance. *Planta*, 241(5), 1109–1118.
- Ernst, W. H. O. (1990). Ecophysiology of plants in waterlogged and flooded environments. *Aquatic Botany*, 38(1), 73–90.
- Finnegan, P. M., & Chen, W. (2012). Arsenic toxicity: The effects on plant metabolism. *Frontiers in Physiology*, 3, 182.
- Foyer, C. H., & Noctor, G. (2012). Managing the cellular redox hub in photosynthetic organisms. *Plant, Cell & Environment*, 35(2), 199–201.
- Gibbs, D. J., Lee, S. C., Isa, N. M., Gramuglia, S., Fukao, T., Bassel, G. W., ... Holdsworth, M. J. (2011). Homeostatic response to hypoxia is regulated by the N-end rule pathway in plants. *Nature*, 479, 415–418.
- Good, N. E. (1977). Uncoupling of electron transport from phosphorylation in chloroplasts. In A. Trebst, & M. Avron (Eds.), *Photosynthesis I: Photosynthetic electron transport and photophosphorylation* (ed., Vol. 5). *Encyclopedia of Plant Physiology, New Series*. (pp. 429–436). Berlin: Springer.
- Hanson, G. T., Aggeler, R., Oglesbee, D., Cannon, M., Capaldi, R. A., Tsien, R. Y., & Remington, S. J. (2004). Investigating mitochondrial redox potential with redox-sensitive green fluorescent protein indicators. *Journal of Biological Chemistry*, 279(13), 13044–13053.
- Hirayama, T., & Shinozaki, K. (2010). Research on plant abiotic stress responses in the post-genome era: Past, present and future. *The Plant Journal*, 61(6), 1041–1052.
- Hughes, M. F. (2002). Arsenic toxicity and potential mechanisms of action. *Toxicology Letters*, 133(1), 1–16.
- IBM Corp. Released 2011. *IBM SPSS Statistics for Windows, Version 20.0*. Armonk, NY: IBM Corp.
- Izarray, R. A., Hobbs, B., Collin, F., Beazer-Barclay, Y. D., Antonellis, K. J., Scherf, U., & Speed, T. P. (2003). Exploration, normalization, and summaries of high density oligonucleotide array probe level data. *Biostatistics*, 4(2), 249–264.
- Isayenko, S. V., & Maathuis, F. J. (2008). The *Arabidopsis thaliana* aquaglyceroporin AtNIP7;1 is a pathway for arsenite uptake. *FEBS Letters*, 582, 1625–1628.
- Islam, E., Khan, M. T., & Irem, S. (2015). Biochemical mechanisms of signaling: Perspectives in plants under arsenic stress. *Ecotoxicology and Environmental Safety*, 114, 126–133.
- Jackson, M. B. (2002). Long-distance signalling from roots to shoots assessed: The flooding story. *Journal of Experimental Botany*, 53, 175–181.
- Johnston, E. J., Rylott, E. L., Beynon, E., Lorenz, A., Chechik, V., & Bruce, N. C. (2015). Monodehydroascorbate reductase mediates TNT toxicity in plants. *Science*, 349, 1072–1075.
- Kataoka, T., Hayashi, N., Yamaya, T., & Takahashi, H. (2004). Root-to-shoot transport of sulfate in *Arabidopsis*. Evidence for the role of SULTR3;5 as a component of low-affinity sulfate transport system in the root vasculature. *Plant Physiology*, 136, 4198–4204.
- Kataoka, T., Watanabe-Takahashi, A., Hayashi, N., Ohnishi, M., Mimura, T., Buchner, P., ... Takahashi, H. (2004). Vacuolar sulfate transporters are essential determinants controlling internal distribution of sulfate in *Arabidopsis*. *The Plant Cell*, 16(10), 2693–2704.
- Klughammer, C., & Schreiber, U. (2016). Deconvolution of ferredoxin, plastocyanin, and P700 transmittance changes in intact leaves with a new type of kinetic LED array spectrophotometer. *Photosynthesis Research*, 128(2), 195–214.
- König, K., Galliard, H., Moore, M., Treffon, P., Seidel, T., & Dietz, K. J. (2014). Assessing redox state and reactive oxygen species in circadian rhythmicity. In *Plant circadian networks* (pp. 239–271). Humana Press, New York, NY.
- Licausi, F., Kosmacz, M., Weits, D. A., Giuntoli, B., Giorgi, F. M., Voeselek, L. A., ... van Dongen, J. T. (2011). Oxygen sensing in plants is mediated by an N-end rule pathway for protein destabilization. *Nature*, 479(7373), 419–422.
- Lichtenthaler, H. K., & Buschmann, C. (2001). Chlorophylls and carotenoids: Measurement and characterization by UV-VIS spectroscopy. *Current Protocols in Food Analytical Chemistry*, F4(3), 1–F4.3.8.
- Lindsay, E. R., & Maathuis, F. J. (2017). New molecular mechanisms to reduce arsenic in crops. *Trends in Plant Science*, 22(12), 1016–1026.
- Ma, Y., Zhu, M., Shabala, L., Zhou, M., & Shabala, S. (2016). Conditioning of roots with hypoxia increases aluminium and acid stress tolerance by mitigating activation of K<sup>+</sup> efflux channels by ROS in Barley: Insights into cross-tolerance mechanisms. *Plant Cell Physiology*, 57, 160–173.



- Maynard, D., Gröger, H., Dierks, T., & Dietz, K. J. (2018). The function of the oxylipin 12-oxophytodienoic acid (OPDA) in cell signaling, stress acclimation and development. *Journal of Experimental Botany*. in press
- Mi, H., Dong, Q., Muruganujan, A., Gaudet, P., Lewis, S., & Thomas, P. D. (2009). PANTHER Version 7: Improved phylogenetic trees, orthologs and collaboration with the Gene Ontology Consortium. *Nucleic Acids Research*, 38, D204–D210.
- Mittler, R. (2002). Oxidative stress, antioxidants and stress tolerance. *Trends in Plant Science*, 7(9), 405–410.
- Mittler, R., Vanderauwera, S., Gollery, M., & Van Breusegem, F. (2004). Reactive oxygen gene network of plants. *Trends in Plant Science*, 9(10), 490–498.
- Motohashi, R., & Myouga, F. (2015). Chlorophyll fluorescence measurements in *Arabidopsis* plants using a pulse-amplitude-modulated (PAM) fluorometer. *Bio-Protocol*, 5(9). e1464
- Noctor, G., Mhamdi, A., Chaouch, S., Han, Y. I., Neukermans, J., Marquez-Garcia, B., ... Foyer, C. H. (2012). Glutathione in plants: An integrated overview. *Plant, Cell & Environment*, 35(2), 454–484.
- Okazaki, Y., & Saito, K. (2014). Roles of lipids as signaling molecules and mitigators during stress response in plants. *The Plant Journal*, 79(4), 584–596.
- Pandey, P., Ramegowda, V., & Senthil-Kumar, M. (2015). Shared and unique responses of plants to multiple individual stresses and stress combinations: Physiological and molecular mechanisms. *Frontiers in Plant Science*, 6, 723.
- Park, S. W., Li, W., Viehhauser, A., He, B., Kim, S., Nilsson, A. K., ... Lawrence, C. B. (2013). Cyclophilin 20-3 relays a 12-oxo-phytyldienoic acid signal during stress responsive regulation of cellular redox homeostasis. *Proceedings of National Academy of Sciences USA*, 110, 9559–9564.
- Poyton, R. O., Ball, K. A., & Castello, P. R. (2009). Mitochondrial generation of free radicals and hypoxic signaling. *Trends in Endocrinology and Metabolism*, 20(7), 332–340.
- Prasch, C. M., & Sonnewald, U. (2015). Signaling events in plants: Stress factors in combination change the picture. *Environmental and Experimental Botany*, 114, 4–14.
- Pucciariello, C., Banti, V., & Perata, P. (2012). ROS signaling as common element in low oxygen and heat stresses. *Plant Physiology and Biochemistry*, 59, 3–10.
- Queval, G., & Noctor, G. (2007). A plate reader method for the measurement of NAD, NADP, glutathione, and ascorbate in tissue extracts: Application to redox profiling during *Arabidopsis* rosette development. *Analytical Biochemistry*, 363(1), 58–69.
- Rabino, I., & Mancinelli, A. L. (1986). Light, temperature, and anthocyanin production. *Plant Physiology*, 81(3), 922–924.
- Rahantaniaina, M. S., Li, S., Chatel-Innocenti, G., Tuzet, A., Issakidis-Bourguet, E., Mhamdi, A., & Noctor, G. (2017). Cytosolic and chloroplastic DHARs cooperate in oxidative stress-driven activation of the salicylic acid pathway. *Plant Physiology*, 174, 956–971.
- Ramakers, C., Ruijter, J. M., Deprez, R. H. L., & Moorman, A. F. (2003). Assumption-free analysis of quantitative real-time polymerase chain reaction (PCR) data. *Neuroscience Letters*, 339(1), 62–66.
- Rasmussen, S., Barah, P., Suarez-Rodriguez, M. C., Bressendorff, S., Friis, P., Costantino, P., ... Mundy, J. (2013). Transcriptome responses to combinations of stresses in *Arabidopsis*. *Plant Physiology*, 161(4), 1783–1794.
- Remy, E., Cabrito, T. R., Batista, R. A., Teixeira, M. C., Sá-Correia, I., & Duque, P. (2012). The Pht1;9 and Pht1;8 transporters mediate inorganic phosphate acquisition by the *Arabidopsis thaliana* root during phosphorus starvation. *New Phytologist*, 195, 356–371.
- Rizhsky, L., Liang, H., Shuman, J., Shulaev, V., Davletova, S., & Mittler, R. (2004). When defense pathways collide. The response of *Arabidopsis* to a combination of drought and heat stress. *Plant Physiology*, 134(4), 1683–1696.
- Romero-Puertas, M. C., Laxa, M., Mattè, A., Zaninotto, F., Finkemeier, I., Jones, A. M., ... Delledonne, M. (2007). S-Nitrosylation of peroxiredoxin II E promotes peroxynitrite-mediated tyrosine nitration. *The Plant Cell*, 19(12), 4120–4130.
- Ruijter, J. M., Ramakers, C., Hoogaars, W. M. H., Karlen, Y., Bakker, O., Van den Hoff, ... Moorman, A. F. M. (2009). Amplification efficiency: Linking baseline and bias in the analysis of quantitative PCR data. *Nucleic Acids Research*, 37(6), e45–e45.
- Saisho, D., Nambara, E., Naito, S., Tsutsumi, N., Hirai, A., & Nakazono, M. (1997). Characterization of the gene family for alternative oxidase from *Arabidopsis thaliana*. *Plant Molecular Biology*, 35, 585–596.
- Sasidharan, R., & Mustroph, A. (2011). Plant oxygen sensing is mediated by the N-end rule pathway: A milestone in plant anaerobiosis. *The Plant Cell*, 23(12), 4173–4183.
- Sauter, A., Dietz, K. J., & Hartung, W. (2002). A possible stress physiological role of abscisic acid conjugates in root-to-shoot signalling. *Plant, Cell & Environment*, 25, 223–228.
- Schmöger, M. E., Oven, M., & Grill, E. (2000). Detoxification of arsenic by phytochelatin in plants. *Plant Physiology*, 122(3), 793–802.
- Schreiber, U. (2017). Redox changes of ferredoxin, P700, and plastocyanin measured simultaneously in intact leaves. *Photosynthesis Research*, 134(3), 343–360.
- Schreiber, U., & Klughammer, C. (2016). Analysis of photosystem I donor and acceptor sides with a new type of online-deconvoluting kinetic LED-array spectrophotometer. *Plant and Cell Physiology*, 57(7), 1454–1467.
- Schwarzländer, M., Fricker, M. D., Müller, C., Marty, L., Brach, T., Novak, J., ... Meyer, A. J. (2008). Confocal imaging of glutathione redox potential in living plant cells. *Journal of Microscopy*, 231(2), 299–316.
- Selinski, J., Hartmann, A., Deckers-Hebestreit, G., Day, D. A., Whelan, J., & Scheibe, R. (2018). Alternative oxidase isoforms are differentially activated by tricarboxylic acid cycle intermediates. *Plant Physiology*, 176, 1423–1432.
- Shabala, S., & Cuin, T. A. (2008). Potassium transport and plant salt tolerance. *Physiologia Plantarum*, 133(4), 651–669.
- Sharma, S. S., & Dietz, K. J. (2009). The relationship between metal toxicity and cellular redox imbalance. *Trends in Plant Science*, 14, 43–50.
- Sharma, S. S., Dietz, K. J., & Mimura, T. (2016). Vacuolar compartmentalization as indispensable component of heavy metal detoxification in plants. *Plant, Cell & Environment*, 39(5), 1112–1126.
- Sharma, S. S., Schat, H., Vooijs, R., & Van Heerwaarden, L. M. (1999). Combination toxicology of copper, zinc, and cadmium in binary mixtures: Concentration-dependent antagonistic, non-additive, and synergistic effects on root growth in *Silene vulgaris*. *Environmental Toxicology and Chemistry*, 18(2), 348–355.
- Sharp, R. E., & LeNoble, M. E. (2002). ABA, ethylene and the control of shoot and root growth under water stress. *Journal of Experimental Botany*, 53, 33–37.
- Shingaki-Wells, R., Millar, A. H., Whelan, J., & Narsai, R. (2014). What happens to plant mitochondria under low oxygen? An omics review of the responses to low oxygen and reoxygenation. *Plant, Cell & Environment*, 37(10), 2260–2277.
- Song, W. Y., Park, J., Mendoza-Cózatl, D. G., Suter-Grotemeyer, M., Shim, D., Hörtensteiner, S., ... Martinoia, E. (2010). Arsenic tolerance in *Arabidopsis* is mediated by two ABCC-type phytochelatin transporters. *Proceedings of National Academy of Sciences USA*, 107(49), 21187–21192.
- Srivastava, M., Ma, L. Q., Singh, N., & Singh, S. (2005). Antioxidant responses of hyper-accumulator and sensitive fern species to arsenic. *Journal of Experimental Botany*, 56(415), 1335–1342.
- Steffens, B., Steffen-Heins, A., & Sauter, M. (2013). Reactive oxygen species mediate growth and death in submerged plants. *Frontiers in Plant Science*, 4, 179.
- Sussmilch, F. C., Atallah, N. M., Brodribb, T. J., Banks, J. A., & McAdam, S. A. (2017). Abscisic acid (ABA) and key proteins in its perception and signaling pathways are ancient, but their roles have changed through time. *Plant Signaling & Behavior*, 12(9), 12862–12867.



- Syvrtsen, J. P., & Garcia-Sanchez, F. (2014). Multiple abiotic stresses occurring with salinity stress in citrus. *Environmental and Experimental Botany*, 103, 128–137.
- Taki, N., Sasaki-Sekimoto, Y., Obayashi, T., Kikuta, A., Kobayashi, K., Aina, T., ... Takamiya, K. I. (2005). 12-Oxo-phytodienoic acid triggers expression of a distinct set of genes and plays a role in wound-induced gene expression in *Arabidopsis*. *Plant Physiology*, 139(3), 1268–1283.
- Thimm, O., Bläsing, O., Gibon, Y., Nagel, A., Meyer, S., Krüger, P., ... Stitt, M. (2004). MapMan: A user-driven tool to display genomics data sets onto diagrams of metabolic pathways and other biological processes. *The Plant Journal*, 37(6), 914–939.
- Thomas, P. D., Campbell, M. J., Kejariwal, A., Mi, H., Karlak, B., Daverman, R., ... Narechania, A. (2003). PANTHER: A library of protein families and subfamilies indexed by function. *Genome Research*, 13(9), 2129–2141.
- Tiew, T. W., Sheahan, M. B., & Rose, R. J. (2015). Peroxisomes contribute to reactive oxygen species homeostasis and cell division induction in *Arabidopsis* protoplasts. *Frontiers in Plant Science*, 6, 658.
- Todgham, A. E., & Stillman, J. H. (2013). Physiological responses to shifts in multiple environmental stressors: Relevance in a changing world. *Integrative and Comparative Biology*, 53(4), 539–544.
- Tu, C., & Ma, L. Q. (2003). Effects of arsenate and phosphate on their accumulation by an arsenic-hyperaccumulator *Pteris vittata* L. *Plant and Soil*, 249(2), 373–382.
- Untergasser, A., Nijveen, H., Rao, X., Bisseling, T., Geurts, R., & Leunissen, J. A. (2007). Primer3Plus, an enhanced web interface to Primer3. *Nucleic Acids Research*, 35(2), W71–W74.
- Upadhyay, R., & Panda, S. K. (2010). Zinc reduces copper toxicity induced oxidative stress by promoting antioxidant defense in freshly grown aquatic duckweed *Spirodela polyrhiza* L. *Journal of Hazardous Materials*, 175(1), 1081–1084.
- Vadassery, J., Reichelt, M., Hause, B., Gershenzon, J., Boland, W., & Mithöfer, A. (2012). CML42-mediated calcium signaling coordinates responses to *Spodoptera* herbivory and abiotic stresses in *Arabidopsis*. *Plant Physiology*, 159, 1159–1175.
- Van Dongen, J. T., Fröhlich, A., Ramírez-Aguilar, S. J., Schauer, N., Fernie, A. R., Erban, A., ... Geigenberger, P. (2008). Transcript and metabolite profiling of the adaptive response to mild decreases in oxygen concentration in the roots of *Arabidopsis* plants. *Annals of Botany*, 103(2), 269–280.
- Vandesompele, J., De Preter, K., Pattyn, F., Poppe, B., Van Roy, N., De Paepe, A., & Speleman, F. (2002). Accurate normalization of real-time quantitative RT-PCR data by geometric averaging of multiple internal control genes. *Genome Biology*, 3(7), research0034–1
- Vernoux, T., Wilson, R. C., Seeley, K. A., Reichheld, J. P., Muroy, S., Brown, S., ... Sung, Z. R. (2000). The ROOT MERISTEMLESS1/CADMIUM SENSITIVE2 gene defines a glutathione-dependent pathway involved in initiation and maintenance of cell division during postembryonic root development. *The Plant Cell*, 12(1), 97–110.
- Wang, F., Chen, Z. H., Liu, X., Colmer, T. D., Shabala, L., Salih, A., ... Shabala, S. (2017). Revealing the roles of GORK channels and NADPH oxidase in acclimation to hypoxia in *Arabidopsis*. *Journal of Experimental Botany*, 68, 3191–3204.
- Wasternack, C., & Strnad, M. (2016). Jasmonate signaling in plant stress responses and development—Active and inactive compounds. *New Biotechnology*, 33, 604–613.
- Ye, J., Coulouris, G., Zaretskaya, I., Cutcutache, I., Rozen, S., & Madden, T. L. (2012). Primer-BLAST: A tool to design target-specific primers for polymerase chain reaction. *BMC Bioinformatics*, 13(1), 134.
- Yemm, E. W., & Willis, A. J. (1954). The estimation of carbohydrates in plant extracts by anthrone. *Biochemical Journal*, 57(3), 508–514.
- Zhao, F. J., McGrath, S. P., & Meharg, A. A. (2010). Arsenic as a food chain contaminant: Mechanisms of plant uptake and metabolism and mitigation strategies. *Annual Review of Plant Biology*, 61, 535–559.
- Zuber, H., Davidian, J. C., Wirtz, M., Hell, R., Belghazi, M., Thompson, R., & Gallardo, K. (2010). Sultr4; 1 mutant seeds of *Arabidopsis* have an enhanced sulphate content and modified proteome suggesting metabolic adaptations to altered sulphate compartmentalization. *BMC Plant Biology*, 10(1), 78.

## SUPPORTING INFORMATION

Additional supporting information may be found online in the Supporting Information section at the end of the article.

**How to cite this article:** Kumar V, Vogelsang L, Seidel T, et al. Interference between arsenic-induced toxicity and hypoxia. *Plant Cell Environ*. 2019;42:574–590. <https://doi.org/10.1111/pce.13441>